Effect of the electric field profile on the accuracy of E-FISH measurements in ionization waves

Tat Loon Chng, David Z. Pai, Olivier Guaitella, Svetlana Starikovskaia, Anne Bourdon

Effect of the Electric Field Profile on the Accuracy of E-FISH Measurements in Ionization Waves

To cite this article before publication: Tat Loon Chng *et al* 2021 *Plasma Sources Sci. Technol.* in press https://doi.org/10.1088/1361-6595/ac4592

Effect of the Electric Field Profile on the Accuracy of E-FISH Measurements in Ionization Waves

Tat Loon Chng[1], David Z. Pai[1], Olivier Guaitella[1], Svetlana M. Starikovskaia[1], Anne Bourdon[1]

[1]*Laboratoire de Physique des Plasmas, (CNRS, Sorbonne Université, Université Paris-Saclay), École Polytechnique, Institut Polytechnique de Paris, F-91128, Palaiseau, France*

Abstract

Electric field induced second harmonic (E-FISH) generation has emerged as a versatile tool for measuring absolute electric field strengths in time-varying, non-equilibrium plasmas and gas discharges. Yet recent work has demonstrated that the E-FISH signal, when produced with tightly focused laser beams, exhibits a strong dependence on both the length and shape of the applied electric field profile (along the axis of laser beam propagation). In this paper, we examine the effect of this dependence more meaningfully, by predicting what an E-FISH experiment would measure in a plasma, using 2D axisymmetric numerical fluid simulations as the true value. A pin-plane nanosecond discharge at atmospheric pressure is adopted as the test configuration, and the electric field evolution during the propagation of the ionization wave (IW) is specifically analyzed. We find that the various phases of this evolution (before and up to the front arrival, immediately behind the front and after the connection to the grounded plane) are quite accurately described by three unique electric field profile shapes, each of which produces a different response in the E-FISH signal. As a result, the accuracy of an E-FISH measurement is generally predicted to be comparable in the first and third phases of the IW evolution, and significantly poorer in the second (intermediate) phase. Fortunately, even though the absolute error in the field strength at certain time instants could be large, the overall shape of the field evolution curve is relatively well captured by E-FISH. Guided by the simulation results, we propose a procedure for estimating the error in the initial phase of the IW development, based on the presumption that the starting field profile mirrors that of its corresponding Laplacian conditions before evolving further. We expect that this approach may be readily generalized and applicable to other IW problems or phenomena, thus extending the utility of the E-FISH diagnostic.

1. Introduction

Electric field induced second harmonic generation or E-FISH [1], is a nonlinear optical phenomenon that has recently been exploited as a laser-based method for measuring electric fields [2-4] in non-equilibrium plasmas [5-18, 36]. The non-resonant nature of the second harmonic generation implies that the signal production is effectively instantaneous with respect to the laser excitation, fundamentally limiting the time response of the interaction to less than a picosecond. This provides the sub-nanosecond time resolution typically required for tracking rapid field changes in these pulsed plasmas.

On a parallel note, the quadratic dependence of the E-FISH signal on the probe beam intensity suggests that the signal should be dominated by contributions from the focal region, where the laser intensity is highest. In other words, the size of the beam focus (characterized by the laser Rayleigh range) defines the measurement resolution, and favours the use of tighter focusing if better spatial resolution is desired. Yet, a more recent study has shown that while the size of the focal region represents a *limit* to the achievable spatial resolution, defining the effective resolution of an E-FISH measurement, especially when *tightly focused* laser beams are used, is a more complex issue. In that study, it was pointed out that, in addition to intensity variations along the axis of beam propagation, *phase variations* also play a crucial role in influencing the signal [19]. The effects of the latter tend to be more subtle, and can lead to results that contradict interpretations reasoned on intensity arguments alone. In particular, the intrinsic phase variations associated with a focused laser beam, also commonly known as the Gouy phase shift [20], can *significantly* influence the signal even when present in the far field (i.e. far beyond the beam focus). It is worth emphasizing that this phenomenon is especially important for nonlinear, coherent optical interactions such as second and third harmonic generation [21], as well as E-FISH [19].

An undesirable (and unintended) consequence of using a focused probe beam is that the E-FISH signal becomes more generally a function of the *entire* applied electric field profile that overlaps with the laser beam path, rather than merely the local field at the beam focus [19,25]. This in turn confounds an absolute field measurement since it requires that the shape of the electric field profile in a plasma be either known beforehand, or be well matched during calibration. Both these requirements are clearly challenging to fulfil given that the shape of the field profile in a plasma not only depends on the discharge geometry, but also often evolves rapidly with time. A further complication is that this signal distortion is a function of the Rayleigh range, and increases as the probe beam is more tightly focused.

An interesting question that remains unanswered is the *extent* to which these signal distortions occur in a plasma, and their corresponding impact on the field measurement accuracy. Although the effect of the shape of the electric field profile on the E-FISH signal has been characterized in [19], the actual change in this profile shape that occurs in a plasma has not been evaluated. We address this issue by applying theoretical ‘corrections’ to electric field profiles of a nanosecond discharge generated by 2D axisymmetric numerical fluid simulations, with a view to predicting what E-FISH would measure in an experiment. We assess the accuracy of E-FISH by comparing the corrected values against the simulations, taking the latter to be the true values.

Gaining insight into the effect of these field profiles on the accuracy of the E-FISH method is therefore the main objective of this work, with the benefit of both previous and future users in mind. Prior to this study, we were particularly motivated by the fact that the existing E-FISH literature has generally yielded plausible results, which suggests that any error due to the effects of beam focusing could be small. Moreover, the simplicity and high field sensitivity of E-FISH merits its continued use, especially if the level of accuracy can be better understood or if any form of data correction can be implemented. Furthermore, the signal loss due to the large phase mismatch when crossing two laser beams (as proposed in [19]) motivate the use of numerical models to characterize and reduce the traditional E-FISH measurement error.

2. Discharge Fluid Model Description

We simulate the dynamics of 2D axisymmetric discharges in air at atmospheric pressure between a high voltage anode pin electrode and a grounded cathode plane. We use the same 2D fluid model as in [29], based on drift-diffusion equations for electrons, positive and negative ions coupled with Poisson's equation in cylindrical coordinates (x, r). Details on the fluid model equations, numerical methods and boundary conditions are given in [29]. As initial condition, a low uniform density of 10^4 cm^{-3} electrons and positive ions in air is considered, to be close to single pulse experiments. In this work, two set-ups and discharge conditions are studied. In both cases, the computational domain is 2.6 cm x 7.52 cm with the same Cartesian grid as in [29]. First, a pulsed voltage with a rise time of 0.5 ns and a voltage plateau of 50 kV is applied to a rod electrode of 200 µm radius ended by a semi-sphere of same radius set at 1.6 cm from a grounded cathode plane. In this high voltage condition with a sharp anode electrode (named "HV case" in the following), a 2D diffuse nanosecond ionization wave propagates from the point anode to the grounded plane. Figure 1(a) shows 2D images of the electric field and electron density for the HV case at different times of the discharge propagation within the gap. In this work, we restrict our analysis to the use of E-FISH for measurements of the axial component of the electric field, E_x, and since the E-FISH signal is insensitive to the overall sign of this field, the absolute value, $|E_x|$, is shown in figure 1(a). At $t = 3.11$ ns, the discharge connects to the grounded plane and has a conical shape with a maximum radius of $r = 7$ mm at an axial distance $x_\mathrm{d} = 3$ mm, where x_d is defined as the axial (x) distance from the tip of the pin electrode. The average propagation velocity of the discharge front in the gap is 5 mm/ns. Similar diffuse discharges have been observed experimentally and numerically as reviewed in [30]. The simulation of the HV case is stopped at $t = 3.49$ ns, when the time step starts decreasing sharply due to the increase of the electron density in the conductive channel formed between both electrodes. Second, a DC voltage of 13 kV is applied to a hyperboloid electrode with a radius of curvature at its tip of 647 microns set at 5 mm from a grounded plane. In this low voltage condition with a blunt anode electrode (named "LV case" in the following), a discharge with a smaller and more constant radius than in the HV case propagates from the pin to the plane as shown in figure 1(b). When the discharge connects to the grounded cathode plane at $t = 7.37$ ns, the maximum discharge radius is about 1 mm in the middle of the inter-electrode gap. (Following [38], the discharge radius is defined as the shielding radius, or the radial distance from the discharge centerline $(r = 0)$ to the location of the maximum in the radial component, $|E_r|$, of the electric field strength.) For the LV case, the average discharge propagation velocity is 0.67 mm/ns and is in good agreement with experimental and numerical studies carried

out in similar conditions as reviewed by [31]. In the LV case, simulations have been performed until $t = 16.9$ ns to study the electric field evolution after the bridging of the gap.

For both set-ups and discharge conditions, we also calculate the Laplacian electric field, by solving the Laplace equation for the same electrode geometry and the DC applied voltage for the LV case and the same applied voltage at a given time for the HV case.

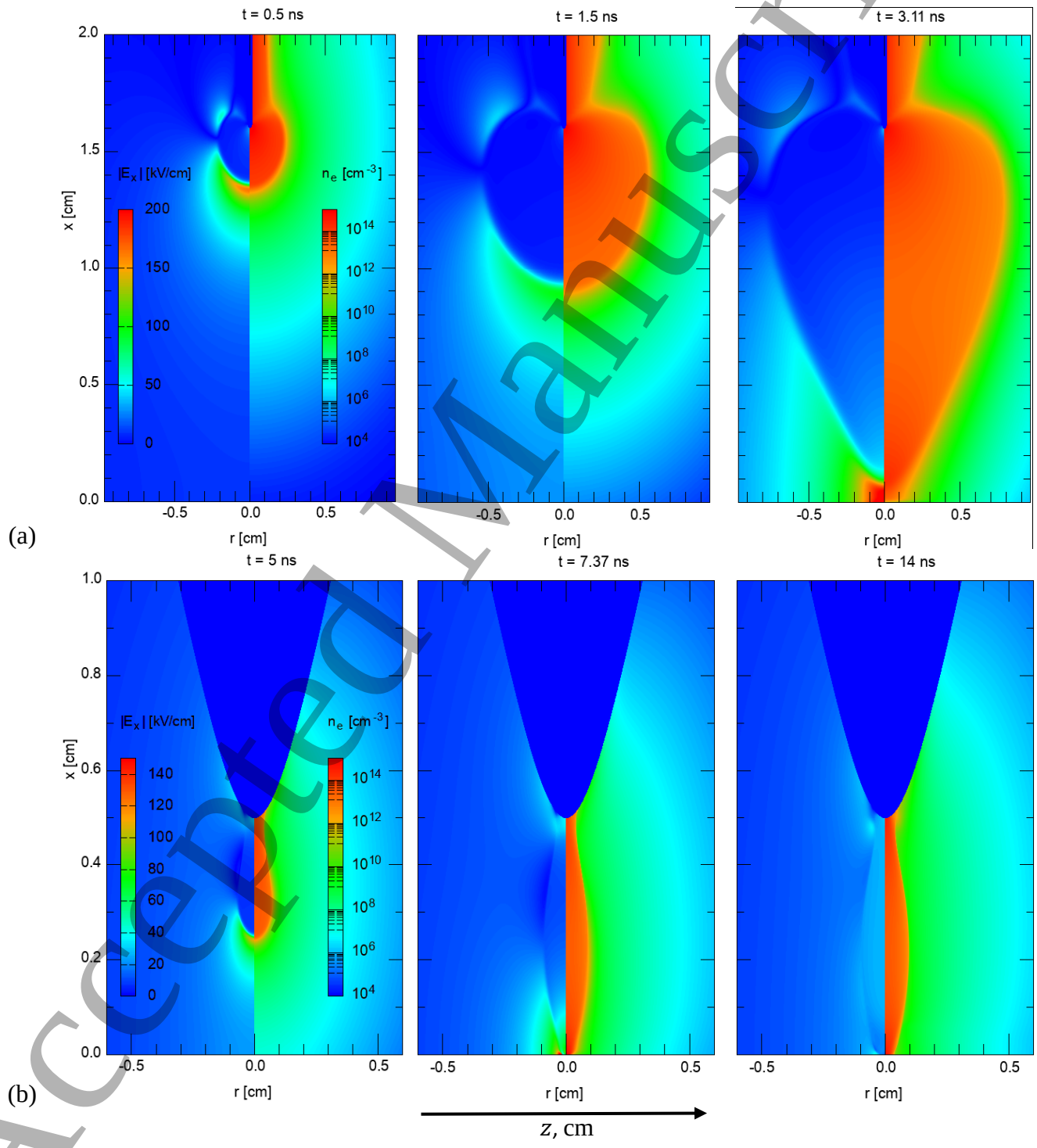

Figure 1. 2D distribution of the axial component of the electric field, $|E_x|$, and electron density, n_e, at 3 different time instants for the (a) HV case, (b) LV case. To avoid confusion, we define a separate z-axis (based on a Cartesian coordinate system) for the direction of laser propagation relevant to the E-FISH calculations. The z-axis therefore spans a distance twice that of the radial axis and both are identical for values of $z \geq 0$.

3. Electric Field Characterization

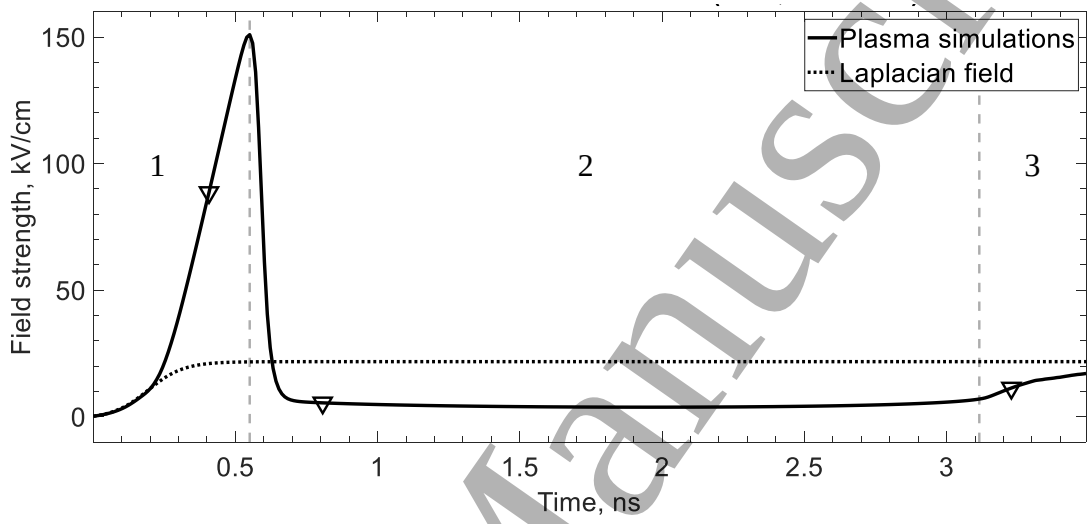

(a)

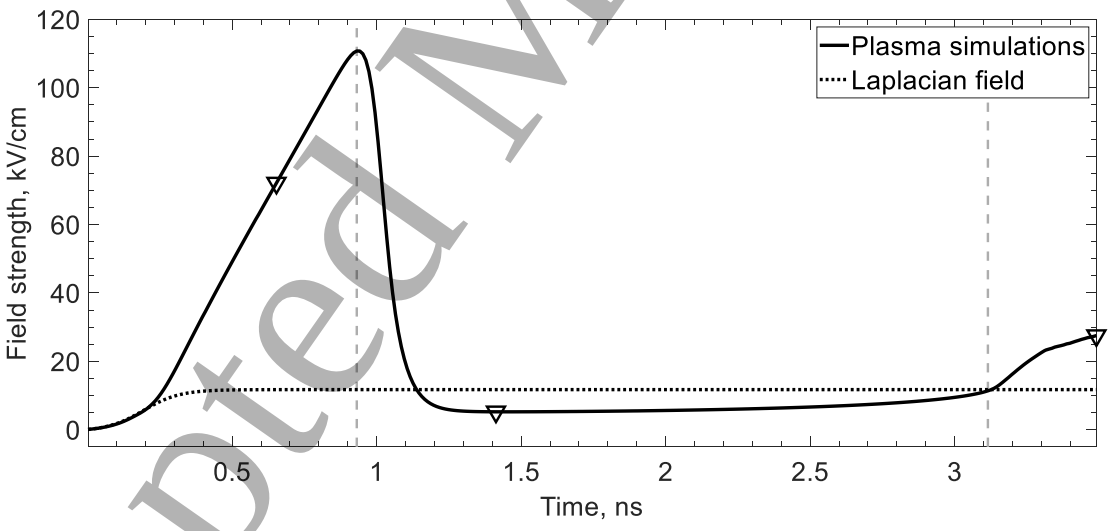

(b)

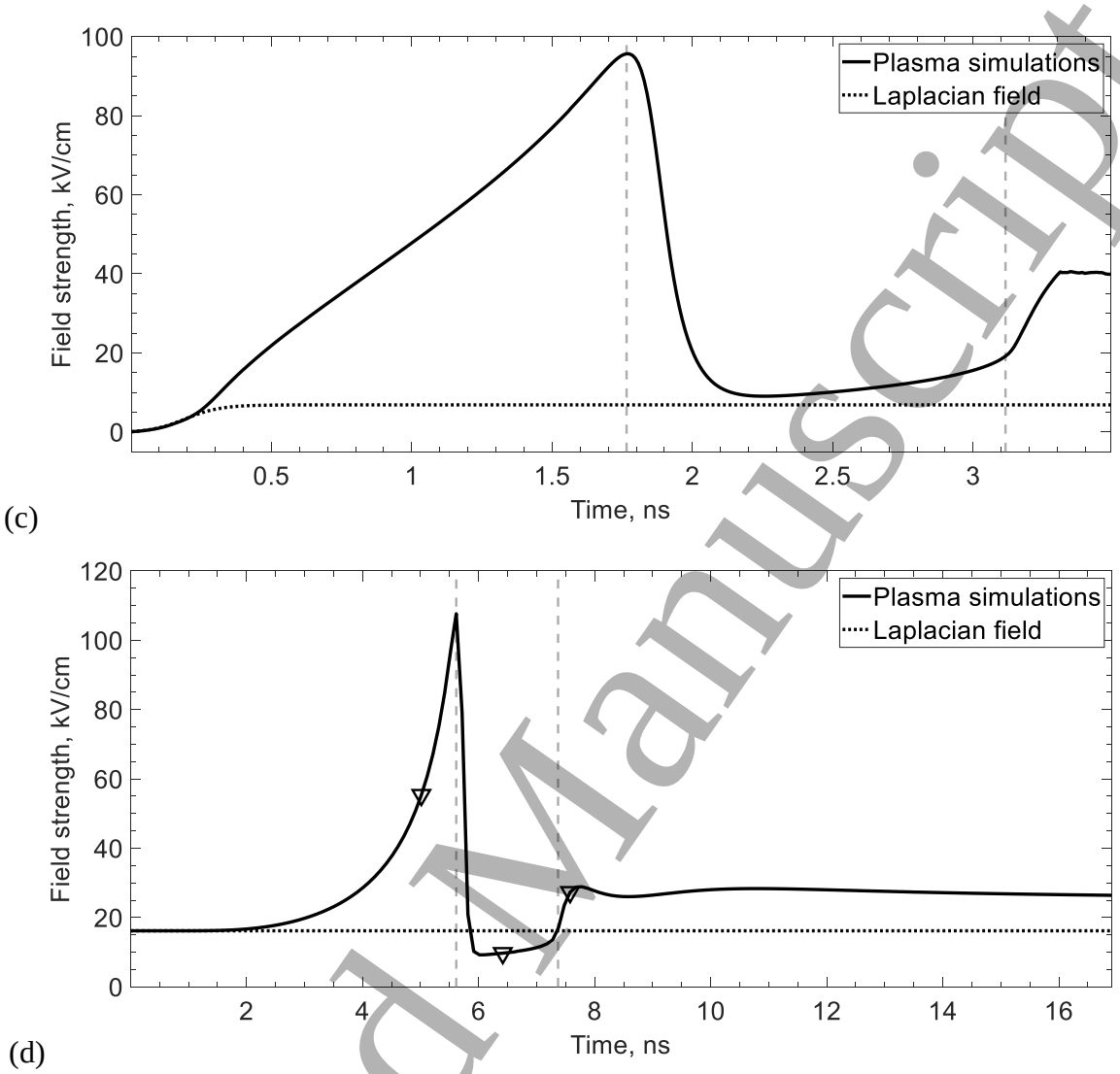

Figure 2. Temporal evolution of the axial component of the electric field, $|E_x|$, for the HV case at various locations along the discharge centerline ($r = 0$) (a) $x_\mathrm{d} = 3$ mm, (b) $x_\mathrm{d} = 5$ mm, (c) $x_\mathrm{d} = 8$ mm and (d) $x_\mathrm{d} = 3$ mm but for the LV case. The grey vertical dashed lines delineate the (time instants of) commencement of phases two and three. Inverted triangles indicate the respective time instants of the z-profiles displayed in figure 3.

Figure 2(a) plots the time evolution of the axial component of the electric field, $|E_x|$, along the discharge or axial centerline (i.e. $r = 0$) at a vertical distance of 3 mm below the pin electrode for an applied voltage of 50 kV. The shape of this time evolution profile exhibits good agreement with existing experimental data, and displays the gross features typical of ionization wave propagation in nanosecond discharges [7, 9, 17, 22-24]. The field strength initially echoes the electrostatic field corresponding to the applied voltage waveform, before displaying a sharp field overshoot that peaks around 150 kV/cm at about $t = 0.55$ ns. This corresponds to the phase of discharge development where the ionization front approaches the point of reference (or measurement). This

is followed by a steep descent in the electric field to about 7 kV/cm after the immediate passage of the wave at around $t = 0.7$ ns, and is due to the charge separation and rapid self-shielding that occurs behind the front. The final phase is characterized by a gentle rise in the field strength as the ionization wave eventually arrives at the plane electrode ($t \approx 3.11$ ns), and the electrons produced in the front start to reach the pin electrode, generating a conduction current. This marks the gradual transition to a quasi-steady state discharge. It is worth mentioning that this chronological description is rather representative of the other x locations along the centerline (as shown in figures 2(b) and 2(c)), and for the simulations with a lower applied voltage of 13 kV (figure 2(d)). The main exceptions are the peak field and the time at which each discharge phase commences. For instance, in comparison with figure 2(a), at $x_\mathrm{d} = 5$ mm and an applied voltage of 50 kV (figure 2(b)), the peak field drops to about 110 kV/cm and is attained at time $t = 0.93$ ns. Similarly, for a lower applied voltage of 13 kV and $x_\mathrm{d} = 3$ mm, the peak field of 107 kV/cm is realized much later at $t = 5.6$ ns. These differences may be readily explained in terms of the proximity of the high voltage electrode to the point of reference, as well as the influence of the applied voltage on the field strength and ionization wave speed.

It is important to reiterate that the path-integrated nature of the E-FISH diagnostic means that the signal is sensitive to the full extent of the electric field profile along the direction of propagation of the laser beam. The time evolution of the electric field, $|E_x|$ plotted in figure 2 tracks the field strength at the *discharge centerline,* $r = 0$. However, in an *equivalent* E-FISH experiment, every data point of a similar such plot (i.e. figure 2) would in fact be a consequence of the *entire* electric field profile along the axis of laser propagation, or the z-axis as defined in figure 1(b). It is therefore of relevance to examine the numerical field profiles along the radial axis. Since the simulations assume axisymmetry, the full spatial extent of the electric field profile along the z-axis is obtained by simply mirroring the radial numerical data about the axial centerline ($r = 0$) at a particular x location. The total length of the z dimension is therefore 15.02 cm, or twice that of the radial axis.

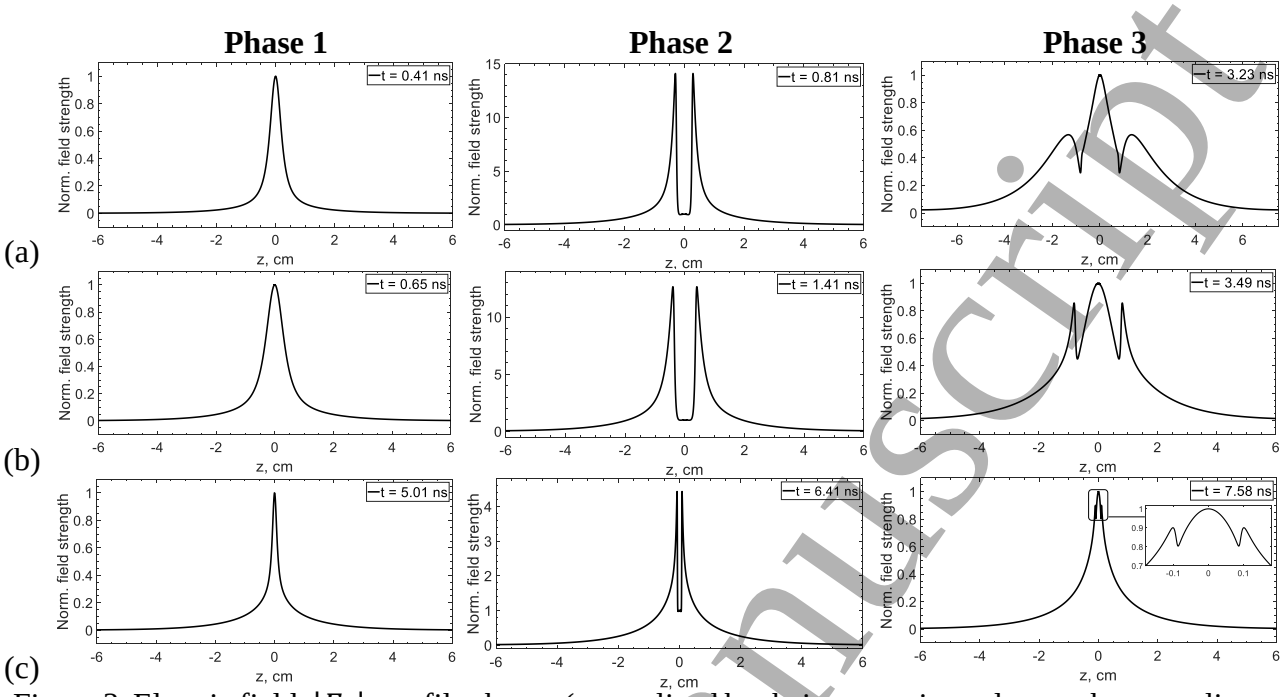

Figure 3. Electric field, $|E_x|$, profile shapes (normalized by their respective values at the centerline, $r = 0$) along the z-axis corresponding to the three distinct phases of the ionization wave evolution. From left to right: bell-shaped profile; double-peak profile; and triple-peak profile. From top to bottom: (a) $x_\mathrm{d} = 3$ mm, (b) $x_\mathrm{d} = 5$ mm (HV case) and (c) $x_\mathrm{d} = 3$ mm (LV case).

Thorough inspection of these individual field profiles along the z-axis reveals a close correspondence between their shapes and the respective phases of the ionization wave evolution. A summary of these most important profiles are provided in figure 3 for various simulated conditions. As shown in the first column, the initial phase is distinguished by a bell-shaped field profile before the arrival of the front and up to the peak value of the electric field. Immediately behind the front (i.e. start of the second phase), this bell-shaped profile begins to evolve into a double-peaked field profile, coinciding with the drop in field strength at the axial centerline ($r = 0$) as seen earlier in figure 2. With further passage of the wave, as this centerline field strength reaches a minimum, these peaks become progressively more pronounced, giving rise to the profiles with a central dip (or 'hole') shown in the second column of figure 3. These z-profiles are indicative of a channel with a low electric field core (and high electron density of about 10^{14} cm^{-3}, see figure 1(a)) surrounded by a skin-like layer of higher field strength, and have also been reported in the literature [18, 32, 33]. In the final phase, after the connection to the grounded plane, as shown in the last column of figure 3, this field dip is replaced by a third peak that gradually increases in strength, yielding a triple-peak shape associated with this field recovery. This suggests the recurrence of a bell-shaped profile as the discharge evolves towards a quasi-steady state, a point we affirm with the aid of the 13 kV computations (see for instance rightmost plot of figure 3(c)), given the longer simulated times. It shall be shown later in section 5 that these three unique electric field shapes, which constitute a fairly complete description of the electric field time evolution, result in very different effects on the E-FISH signal.

4. E-FISH Governing Equations

Following [19], the power of the E-FISH signal for a focused probe beam is given by:

$$P^{(2\omega)} \propto \left[\alpha^{(3)} \cdot N \cdot P_{\mathrm{o}}^{(\omega)}\right]^2 \cdot \left(\frac{1}{z_{\mathrm{R}}}\right) \cdot \left| \int_{-\infty}^{\infty} E_{\mathrm{ext}}(z) \cdot \frac{\exp(\mathrm{i} \cdot \Delta k \cdot z)}{\left[1 + \mathrm{i} \cdot \left(\frac{z}{z_{\mathrm{R}}}\right)\right]} \mathrm{d}z \right|^2 \quad (1)$$

where $\alpha^{(3)}$ is the third-order nonlinear hyperpolarizability (a fourth rank tensor), N is the gas number density, $P_{\mathrm{o}}^{(\omega)}$ is the power of probe beam, z_{R} is the laser Rayleigh range, $E_{\mathrm{ext}}(z)$ is the externally applied electric field distribution along the z-axis, Δk is the wave-vector mismatch, and z is the beam propagation axis as described in section 3. To be precise, the E-FISH signal acquires a polarization that is parallel to that of the external electric field, $E_{\mathrm{ext}}(z)$ [6, 34]. As mentioned earlier in section 2, since our analysis is restricted to the *axial* component of the external electric field, E_x, it should therefore be understood that this produces a polarization of the E-FISH signal that is parallel to the x-axis. For convenience, we drop the subscript 'x' throughout the paper when referring to the external field and the E-FISH signal polarization, even though its meaning (i.e. $P^{(2\omega)} = P_x^{(2\omega)}$ and $E_{\mathrm{ext}} = E_{\mathrm{ext}_x}$) is implied.

The integral on the r.h.s. of equation (1) may be appropriately non-dimensionalized by E_o and z_{R}, giving:

$$P^{(2\omega)} \propto \left[\alpha^{(3)} \cdot N \cdot P_{\mathrm{o}}^{(\omega)}\right]^2 \cdot {E_{\mathrm{o}}}^2 \cdot z_{\mathrm{R}} \cdot \left| \int_{-\infty}^{\infty} {E_{\mathrm{ext}}}'(z') \cdot \frac{\exp(\mathrm{i} \cdot u \cdot z')}{[1 + \mathrm{i} \cdot (z')]} \mathrm{d}z' \right|^2 \quad (2)$$

where

$${E_{\mathrm{ext}}}'(z') = \frac{E_{\mathrm{ext}}(z)}{E_{\mathrm{o}}}, \quad z' = \frac{z}{z_{\mathrm{R}}}, \quad u = \Delta k \cdot z_{\mathrm{R}}$$

and E_{o} is defined as the electric field strength at $z = 0$. We emphasize the distinction between ${E_{\mathrm{ext}}}'(z')$, which is a dimensionless electric field profile, with the actual field shape, $E_{\mathrm{ext}}(z)$.

Rewriting equation (1) in this way allows the effects of the shape of the electric field profile, ${E_{\mathrm{ext}}}'(z')$ and optical parameters such as the wave-vector mismatch, Δk and Rayleigh range, z_{R} to be fully captured by the non-dimensional integral on the r.h.s of equation (2). This also mathematically highlights the problem with the E-FISH diagnostic – that the signal is in fact dependent on two unknown parameters, rather than just one. The first is the electric field at the beam focus, E_{o} (i.e. the quantity of interest), the other being the shape of this *entire* electric field profile, ${E_{\mathrm{ext}}}'(z')$. More importantly, we point out that if this non-dimensional integral on the r.h.s of equation (2), (defined later as the E-FISH modification factor, and captured in figure 4) remains acceptably constant, then the effects of ${E_{\mathrm{ext}}}'(z')$ on the E-FISH signal may be neglected, and the problem reverts to a single unknown. This of course assumes that all other variables in equation (2) including Δk and z_{R}, as well as the terms in the square bracket, remain constant during an experiment.

For convenience, we further define:

$$\Gamma = \left| \int_{-\infty}^{\infty} E_{\text{ext}}'(z') \cdot \frac{\exp(\mathrm{i} \cdot u \cdot z')}{[1 + \mathrm{i} \cdot (z')]} \mathrm{d}z' \right|, \tag{3}$$

where Γ is designated as a modification factor that provides a relative measure of the E-FISH measurement accuracy. It is evident from equation (3) that the value of this modification factor is also strongly dependent on the non-dimensional parameter $u = \Delta k \cdot z_{\mathrm{R}}$. In an E-FISH experiment where Δk is typically constant with time, a variation in u is equivalent to a change in the beam focusing, or z_{R}.

5. Evaluation of E-FISH Measurement Accuracy from Numerical Simulations

The above sections highlight the importance of analyzing the temporal behaviour of the E-FISH modification factor, Γ, in order to understand the corresponding accuracy of the electric field evolution curves given in figure 2. A flat response curve implies that the effects of the electric field profile shape can be safely neglected without any detriment to the measurement accuracy, while large fluctuations in Γ would indicate the exact opposite.

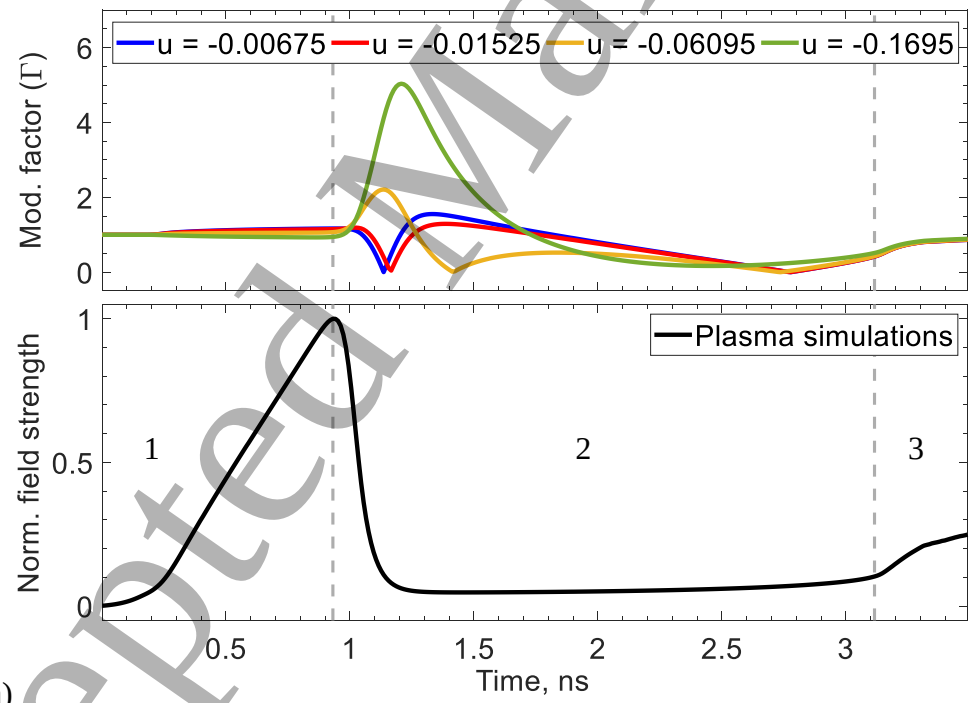

(a)

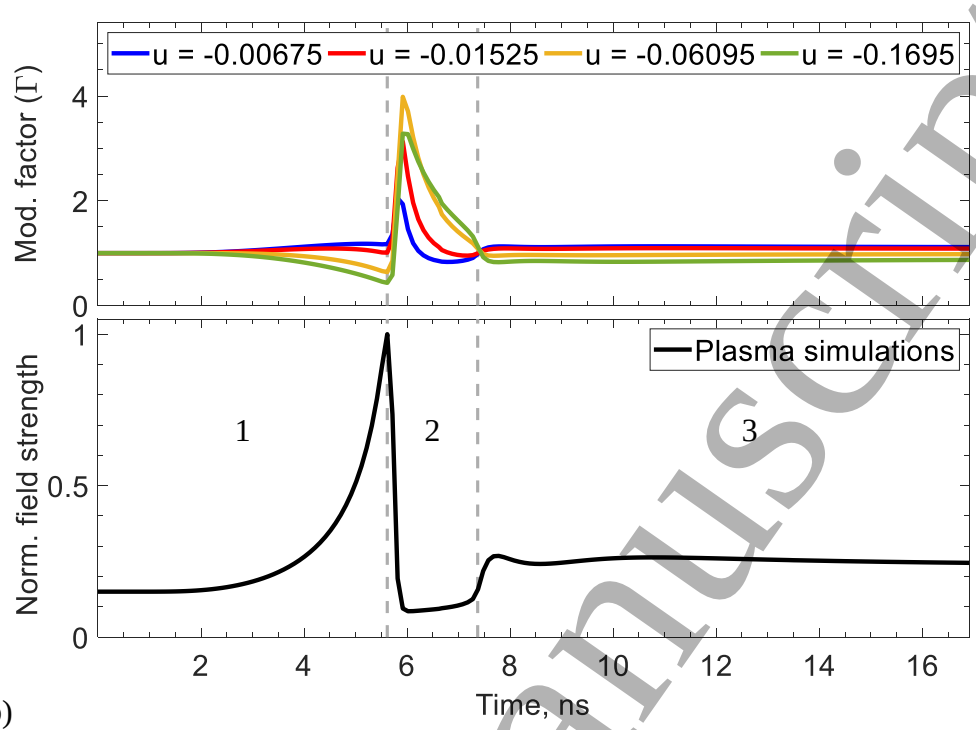

(b)

Figure 4. Top panel: Temporal evolution of the E-FISH modification factor, Γ, computed from electric field profiles along the z-axis, $E_{\mathrm{ext}}{}'(z')$ for four different u. (a) $x_{\mathrm{d}} = 5$ mm, HV case; (b) $x_{\mathrm{d}} = 3$ mm, LV case. For ease of reference, the peak-normalized field evolution curves are included in the bottom panels of each plot. The value of Γ is normalized by its initial value (at $t = 0$) for each u.

Figure 4(a) plots the time evolution of Γ for the conditions of the HV case with $x_{\mathrm{d}} = 5$ mm (figure 2(b)) for different values of the non-dimensional parameter, $u = \Delta k \cdot z_{\mathrm{R}}$. These calculations essentially take into account the effect of the field shapes discussed earlier in figure 3. Both the grid resolution and size of the numerical domain are verified to be sufficiently large such that they have no impact on these calculations of Γ based on equation (3). The values of u are chosen to be consistent with a wave vector mismatch, $\Delta k = -0.5\ \mathrm{cm}^{-1}$ and Rayleigh ranges, $z_{\mathrm{R}} = 0.0135\ \mathrm{cm}, 0.0305\ \mathrm{cm}, 0.122\ \mathrm{cm}$, and $0.339\ \mathrm{cm}$. Δk is calculated based on fundamental and second harmonic wavelengths of 1064 nm and 532 nm in air, with the indices of refraction calculated at room temperature and pressure. The four values of z_{R} correspond to estimates for four typical focal length lenses (f = 10 cm, 15 cm, 30 cm and 50 cm respectively), based on an initial (unfocused) beam waist of 5 mm, and a probe laser wavelength of 1064 nm. The effect of any field variation along the x-axis within the focal beam diameter is found to have a negligible influence on the E-FISH predictions of the electric field evolution, and as such has not been considered in this work. It is interesting to note that even for the same field shape, $E_{\mathrm{ext}}{}'(z')$, a change in u alters both the magnitude and the shape of the modification factor curves. In particular, compared with the second phase of the ionization wave evolution characterized by a sharp fall in the field strength, relatively flatter Γ profiles are observed during the initial and final phases of development. This trend in the E-FISH modification factor is also observed in figure 4(b) for the

conditions of the LV case at $x_d = 3$ mm (figure 2(d)), and is found to be representative of the remaining simulated cases.

However, since Γ is only a relative indicator, an appropriate point of reference or calibration needs to be defined before any conclusive statement on the measurement accuracy can be made. We take advantage of the idea that prior to initiation, the electric field of a discharge is often fully described by solving Laplace's equation for the electrostatic potential of the system (i.e. 'Laplacian field'). Although it is acknowledged that this statement may not always be true – for instance, in the presence of residual charges – the Laplacian field provides a convenient (though not necessarily exclusive) reference point that can be easily accessed by both computation and experiment. It is also a common practice of E-FISH-related studies to rely on an electrostatic field for calibration.

Selecting the Laplacian field as the reference point means that the electric field during these nascent stages of the discharge are designated as 100% accurate (with respect to the influence of the plasma field profile), and the E-FISH modification factor can be evaluated with respect to its value at these initial conditions. A larger Γ compared to its reference value indicates that an E-FISH measurement will result in an over-prediction, while a smaller value implies that the true field strength will be under-predicted. Returning to figure 4, this implies that the effects of the field shape on the E-FISH signal are much less significant in the first and final phases, and therefore the accuracy during these two phases is deemed to be much better than in the second phase. We attribute this primarily to the precise field shape $E_{ext}{}'(z')$ associated with the second, intermediate phase of the wave evolution.

We find that the E-FISH signal responds in a rather complex manner for field distributions with a localized minimum centered near the beam focus, akin to the double peak profiles displayed in figure 3. For these cases, even though the signal is positively correlated with the field strength at the beam focus, this response is not always linear and depends strongly on the value of u, as well as other parameters such as the respective magnitudes of the field peak and field minimum, the width of the field peak, and the spacing between the two peaks. Furthermore, when this local field drop becomes sufficiently large, rather than continuing to decrease, the E-FISH signal instead reverses in trend and starts to increase. This counter-intuitive behaviour is similar to results reported in [19], which have shown that the presence of a field null near the beam focus can lead to a substantial increase in the E-FISH signal versus the case when such field minima are absent. An additional complication is that since the E-FISH signal retains partial sensitivity to the applied electric field beyond the focal region, field profiles that are peaked away from the centerline – such as these double peak profiles – can result in a higher signal even for the same field at the beam focus. The net result is that the E-FISH signal can either over or under predict the true field strengths for different values of u as found in figure 4. The disagreement becomes more pronounced as the difference between the peak field strength and its value at the centerline increases.

The analysis is much less convoluted in the case of phases one and three, which mostly exhibit profiles that are peaked along the centerline (i.e. first and last columns of figure 3). Such field shapes are less susceptible to signal contributions from the laser far field, since the external electric field in these regions are relatively weaker. Less erroneous signal is therefore spatially integrated

in comparison with phase two. The response of the E-FISH modification factor – and therefore accuracy – in phase three becomes increasingly comparable to that of phase one, as the magnitude of the central maximum grows progressively relative to the two adjacent peaks. This is not unexpected since the field profile is effectively reverting to a bell shape associated with phase one. The relative accuracy of these three different phases finds some agreement with the results of a recent study that has compared the (uncorrected) E-FISH experimental data with simulations [35] for a pin-plane geometry. In that study, the largest discrepancies between measurements and simulation were noted to occur during the second phase.

Mathematically, the E-FISH signal corresponding to the Laplacian field shape, ${E_{\mathrm{ext}}}'(z')_{\mathrm{L}}$, for an electric field strength, E_o, of unity, may be inferred from equations (2) and (3) as:

$$P^{(2\omega)}{}_{\mathrm{L}} \propto \left[\alpha^{(3)} \cdot N \cdot P_{\mathrm{o}}^{(\omega)}\right]^2 \cdot z_{\mathrm{R}} \cdot \left| \int_{-\infty}^{\infty} {E_{\mathrm{ext}}}'(z') \cdot \frac{\exp(\mathrm{i} \cdot u \cdot z')}{[1 + \mathrm{i} \cdot (z')]} \mathrm{d}z' \right|^2 = \left[\alpha^{(3)} \cdot N \cdot P_{\mathrm{o}}^{(\omega)}\right]^2 \cdot z_{\mathrm{R}} \cdot {\Gamma_{\mathrm{L}}}^2 \quad (4)$$

where the subscript 'L' denotes the Laplacian electric field and all other terms are as previously defined. This signal is essentially identical to the calibration constant, C, that would be measured in a regular E-FISH experiment, i.e. $P^{(2\omega)}{}_{\mathrm{L}} = C$, when performing calibration in a Laplacian field. Since the Laplacian field profile, ${E_{\mathrm{ext}}}'(z')_{\mathrm{L}}$, is *independent* of E_o, calibration can be performed for different applied field strengths (or voltages), as has typically been done previously, without any loss of accuracy, while reducing the random uncertainty of C. Although it is assumed here that ${E_{\mathrm{ext}}}'(z')_{\mathrm{L}}$ (and therefore $P^{(2\omega)}{}_{\mathrm{L}}$) is defined with respect to the working discharge geometry, it is still in principle, possible to conduct calibration in a different set-up (defined by a separate Laplacian field profile ${E_{\mathrm{ext}}}'(z')_{\mathrm{L''}}$). This is provided that both ${E_{\mathrm{ext}}}'(z')_{\mathrm{L}}$ and ${E_{\mathrm{ext}}}'(z')_{\mathrm{L''}}$ are known, for example via electrostatic simulations, in which case corrections to the measured signal (from the different calibration set-up) can be implemented to retrieve $P^{(2\omega)}{}_{\mathrm{L}}$ for the working geometry. Such an option could prove useful should there be a need to perform calibration in a set-up that produces an electrostatic field profile that is closer to an anticipated plasma field profile.

It follows from the above that the electric field strength corresponding to an arbitrary E-FISH signal (acquired for instance, in a plasma), is given by:

$$(E_{\mathrm{o}})_{\mathrm{meas}} = \sqrt{\frac{P^{(2\omega)}}{P^{(2\omega)}{}_{\mathrm{L}}}} = \frac{\left| \int_{-\infty}^{\infty} E_{\mathrm{ext}}(z')_{\mathrm{true}} \cdot \frac{\exp(\mathrm{i} \cdot u \cdot z')}{[1 + \mathrm{i} \cdot (z')]} \mathrm{d}z' \right|}{\left| \int_{-\infty}^{\infty} {E_{\mathrm{ext}}}'(z')_{\mathrm{L}} \cdot \frac{\exp(\mathrm{i} \cdot u \cdot z')}{[1 + \mathrm{i} \cdot (z')]} \mathrm{d}z' \right|} = (E_{\mathrm{o}})_{\mathrm{true}} \cdot \left(\frac{\Gamma}{\Gamma_{\mathrm{L}}}\right) \quad (5)$$

where the subscripts 'meas' and 'true' refer to the measured and true values respectively. The former refers to the field strength measured directly from an E-FISH experiment (i.e. as a consequence of neglecting the exact electric field profile), while the latter is the true, or actual field strength, in this case, from the simulations. In line with the foregoing discussion, equation (5) provides mathematical proof that the accuracy of an arbitrary E-FISH measurement is directly influenced by the ratio of the modification factor at that point of interest, to its corresponding value in a Laplacian field.

Based on equation (5), figures 5(a)(i) and 5(b)(i) plot the measured field strengths, $(E_o)_{\text{meas}}$, as a function of different u for the 50 kV and 13 kV simulations at two selected axial locations, namely $x_{\text{d}} = 5$ mm and 3 mm respectively. As one might expect from the corresponding results in figure 4, for a particular u, the largest deviations from the true values occur during the sharp drop in field strength, i.e. phase two of the discharge development. However, since these fields are much weaker than their respective peaks, the overall effect on the shape of the evolution curves is less obvious. As evidenced by figures 5a(ii) and 5b(ii), it is encouraging to note that the measured field evolution shapes are largely consistent with their true shape. This could be a possible reason why existing studies have produced plausible results. In other words, even though the absolute field strengths at certain time instants (for instance, phase two) could be in substantial error, these values are often quite low compared with the peak field such that their impact on the field evolution shape significantly less evident.

In terms of the absolute field strengths, and particularly for phase one, we note that the overall E-FISH accuracy (as a function of u) for the LV case simulations are generally poorer than for the HV case; a point we revisit later in section 6. Even then, for all the 13 kV simulations, it is still possible to find a value of u that produces an error of less than 10% (for phase one), as seen in the specific case of figure 5b(i) for $u = -0.01525$.

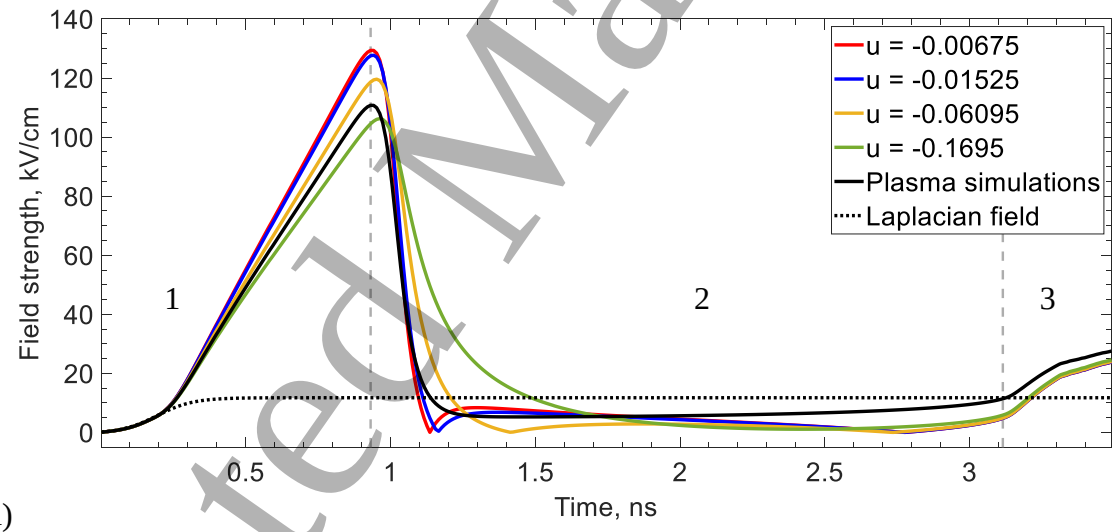

(a)(i)

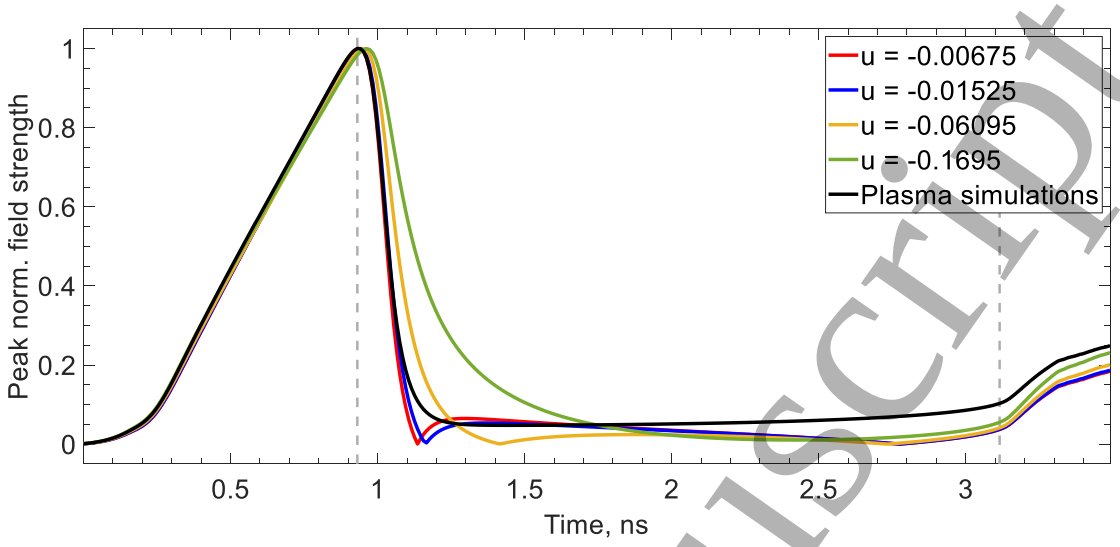

(a)(ii)

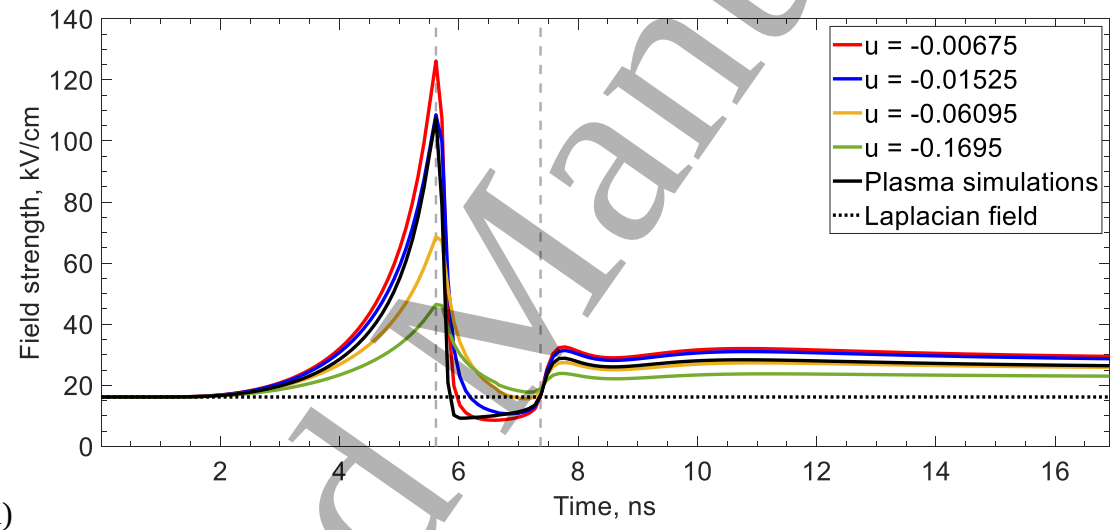

(b)(i)

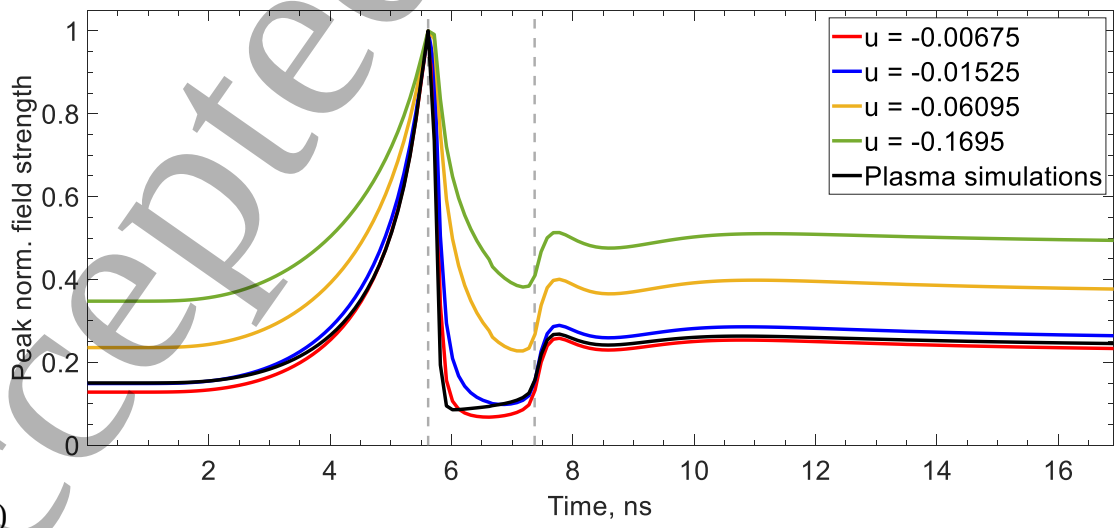

(b)(ii)

Figure 5. Measured (E-FISH) versus true (simulation) electric field evolution profiles for different u. (a) $x_{\mathrm{d}} = 5$ mm, HV case; (b) $x_{\mathrm{d}} = 3$ mm, LV case (i) Absolute values. (ii) Peak-normalized values.

5.1 Implications of the Measurement Accuracy of the Different Discharge Phases

The preceding section has identified phases one and three as the periods of ionization wave development which are likelier to have a better E-FISH accuracy, while phase two tends to perform more poorly. This is especially valuable in the case of phase one, given there are very few techniques that can reliably measure the electric field within this regime. Knowledge of the electric field before the passage of the wave and up to its peak value is important for spatiotemporal characterization of ionization activity in the front, and experimental data is highly sought after for validating numerical simulations. In addition to being compatible with a wide variety of gases [2], the E-FISH diagnostic produces good signals even under conditions of extremely low preionization, and is not constrained by uncertainties regarding the locality of the electron energy distribution function [39,40]. These issues may prove challenging for methods such as line intensity ratio OES, which has generally been limited to N_2 plasmas, even though such challenges have been recently addressed [41-43]. The presence of large spatial gradients in the electric field strength associated with this phase also reduces the effectiveness of capacitive detectors, which have limited spatial resolution, and are restricted only to the longitudinal component of the field vector.

Phase three is of more practical importance as it primarily decides the plasma chemistry. It is the most energetic phase, i.e. energy delivered to the plasma is maximum, since it occurs after the discharge gap is closed and a conductive current begins to flow. Yet in comparison with phase one, the prognosis for characterizing the electric field in this phase is more favourable. Capacitive detectors, for instance, are able to provide good measurements of the field strength, given the more uniform electric field distribution behind the front. In N_2 or air plasmas, the OES method is also more forgiving in this phase especially if the specific deposited energy (i.e. energy delivered to the plasma per particle) is small (≤ 0.1 eV/molecule), and indirect population of the second positive and first negative systems of N_2 is minimal.

The above suggests that the larger errors associated with phase two, which is an intermediate phase possessing characteristics of phases one and three, could be less critical, since its influence on the ionization behaviour in the front and the plasma chemistry is relatively benign.

6. Estimation and Optimization of E-FISH Measurement Accuracy (in Phase One)

While the previous section provides a detailed approach to quantifying and explaining the possible errors that may occur in an E-FISH measurement, these conclusions have been inferred on the premise that the electric field profiles, $E_{\mathrm{ext}}{}'(z')$, are available. In an experiment, only Γ_{L}, the E-FISH modification factor based on the Laplacian field, is expected to be known, but not the value of Γ at any arbitrary time instant during the discharge. In this section, we ask whether it is possible to apply some of the insight acquired in the previous sections towards understanding the accuracy of an E-FISH experiment, more generally, when simulation results are not available.

The need to have sound knowledge of $E_{\mathrm{ext}}{}'(z')$ in order to make an accurate E-FISH measurement appears somewhat contradictory to the very purpose of this diagnostic, which is, in the first place, to measure electric fields. A slight concession to this conflicting requirement is that only the normalized field profiles, $E_{\mathrm{ext}}{}'(z')$, and not the actual field profiles, $E_{\mathrm{ext}}(z')$, need to be known with good accuracy. Furthermore, it is the accuracy of the shape of these field profiles that matters, rather than the exact time instants at which they occur. Nonetheless, we acknowledge that it is a challenging task to predict the shape or behaviour of these field profiles at any point within the discharge.

In view of the above, we single out the *first phase* of the ionization wave development, i.e. before the front passes the reference (or measurement) point, for further analysis. The main rationale for examining this regime are its predictability and ease of characterization. One notes that unlike the remaining two phases of the wave evolution, the initial conditions of the first phase are definitively characterized by the Laplacian field. Hence, more is known about the electric field during this first phase compared with the other two. Furthermore, the evolution of the single-peak, bell-shaped profile associated with this phase, is much easier to characterize than the double and triple peak structures observed in the second and third phases.

A few noteworthy observations emerge upon examination of the field profiles associated with phase one. The first is that these bell-shaped profiles are consistently very well-approximated by the following function:

$$E_{\mathrm{ext}}{}'(z') = \frac{1}{1+\left|\frac{z'}{a'}\right|^{b}};\ \text{and}\ a' = \frac{a}{z_{\mathrm{R}}}. \tag{6}$$

The parameter a' defines the half width at half maximum (i.e. HWHM) of the field profile, a, normalized by z_{R}, while b controls the slope of the profile at the half maximum points (see figure 6). This (membership) function has its origins in fuzzy logic [26], and in the special case of $b = 2$, corresponds to the well-known Lorentzian or Cauchy function. Replacing the electric profiles $E_{\mathrm{ext}}{}'(z')$, obtained from the simulations with these analytical fits produces an agreement in the predicted field strength to within a few percent. The significance of being able to accurately describe $E_{\mathrm{ext}}{}'(z')$ analytically shall become apparent in the following section.

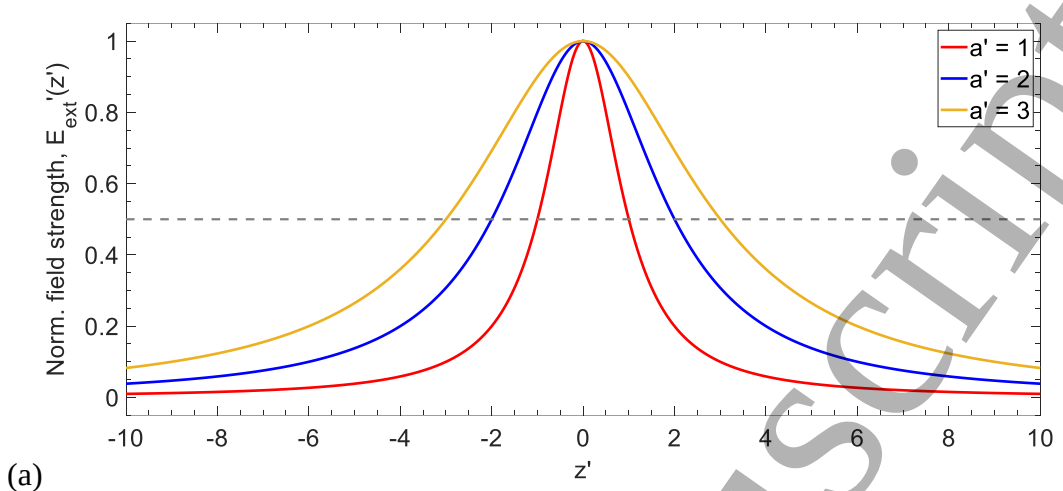

(a)

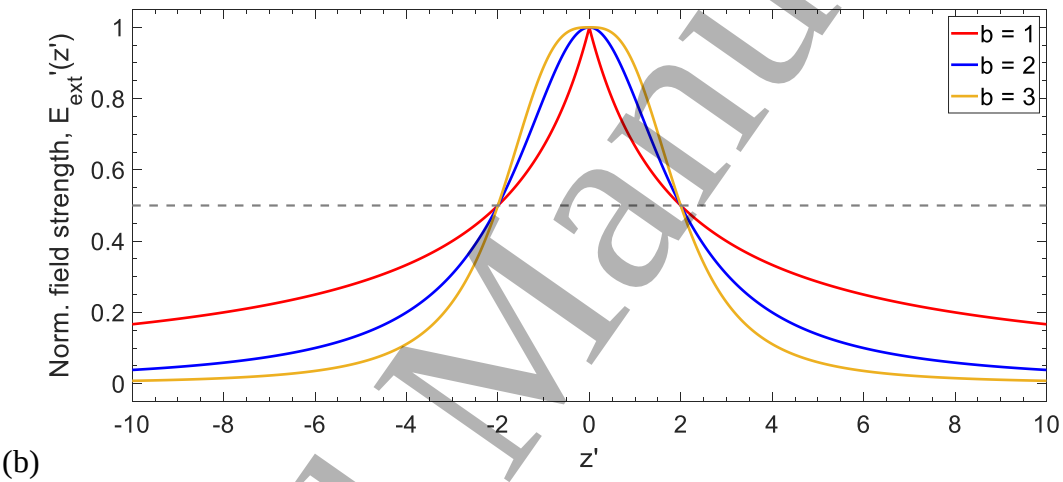

(b)

Figure 6. Effect of the parameters a' and b on the bell-shaped field profile, $E_{\text{ext}}{}'(z')$, for (a) a constant value of $b = 2$, (b) a constant value of $a' = 2$. Increasing a (or a') enlarges the characteristic width of the profile, while increasing b makes the profile 'fatter', approaching a step function in the limit of infinity. The grey dashed horizontal line in each plot denotes the vertical half-maximum.

In addition, the change in the field profile as the field strength grows from its initial Laplacian value to its global maximum, is observed mainly to be in terms of its width, i.e. the parameter a. The parameter b, on the other hand, rises slightly from its initial value, but this variation is found to have a minimal effect on the E-FISH accuracy ($\lesssim 8\%$), and is neglected in our subsequent analysis.

In essence, within this first phase of discharge activity, the bell-shaped, analytical form of $E_{\text{ext}}{}'(z')$ is largely preserved compared to its initial profile. This is not unexpected since the field at any given point within the discharge gap may be treated as an electrostatic problem involving a localized region of space charge (viz. front) moving towards that point. Furthermore, we remark crucially that the width of $E_{\text{ext}}{}'(z')$ also always tends to shrink with time, i.e. a decreases monotonically as shown throughout figure 7. This development appears to be universally valid, with the exception of the Laplacian phase, where the field width expectedly remains unchanged

for reasons earlier mentioned. Likewise, the corresponding duration of this phase for the 50 kV and 13 kV cases ($t_L \approx 0.2$ ns & 0.8 ns respectively), also remains constant across all the different x locations.

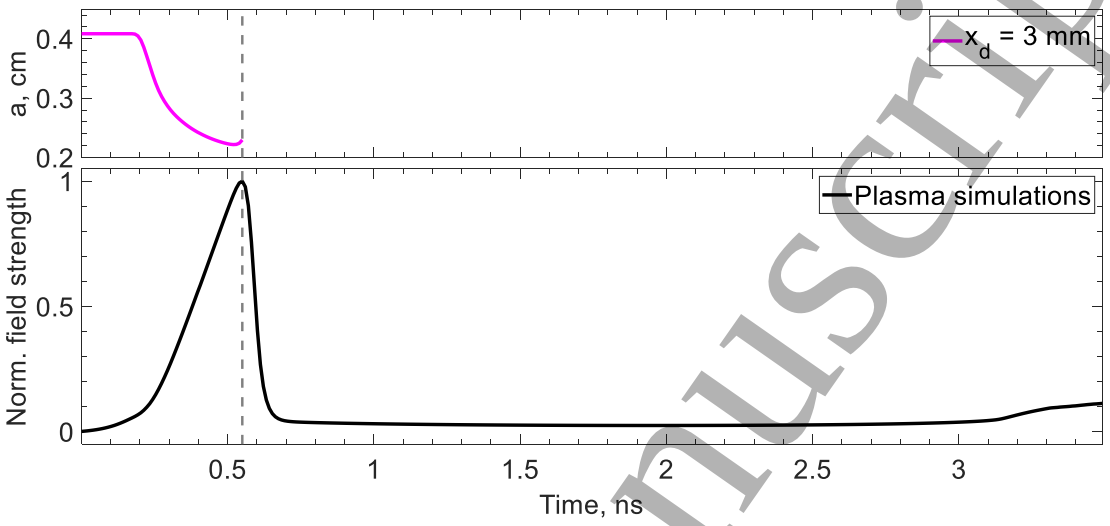

(a)

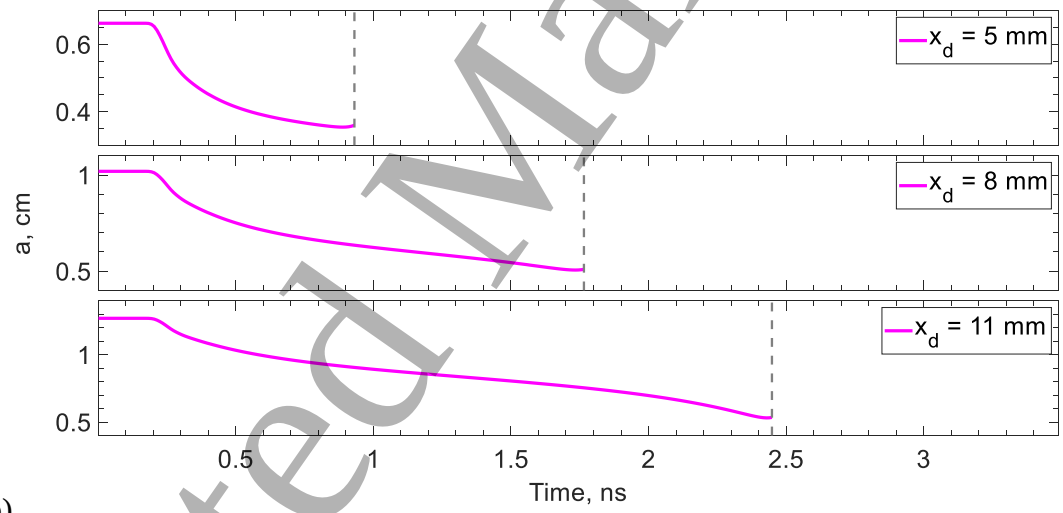

(b)

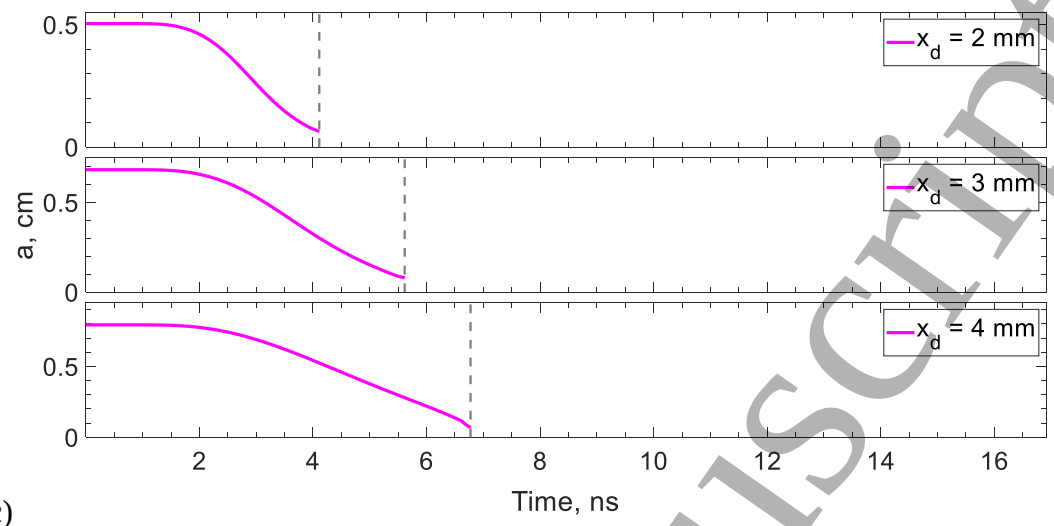

(c)

Figure 7. Time evolution of the field profile half widths, a, at various axial locations below the high voltage pin electrode. (a) $x_{\mathrm{d}} = 3$ mm, HV case. To emphasize that only the first phase of the field evolution is considered, we include the peak normalized field strength in the bottom panel for reference, together with a vertical grey dashed line indicating the termination of the first phase. (b) $x_{\mathrm{d}} = 5$ mm, 8 mm and 11 mm, HV case, and (c) $x_{\mathrm{d}} = 2$ mm, 3 mm and 4 mm, LV case. Note that the duration of phase one increases as one moves further away from the pin. The initial plateau in a is indicative of the Laplacian phase.

Given that this trend of decreasing profile (half) width is common to all the simulated cases, we postulate that this may be explained more generally by a straightforward electrostatics analysis, rather than being attributable to a more complex or specific feature of the discharge evolution. If one may approximate the ionization front as an infinitesimal region of charge density moving towards a reference line (or plane) x, any particular z location (along this line) compared with the origin (i.e. $z = 0$) experiences a relatively smaller increase in field strength with time. This is because the reduction in the (radial) displacement from the front to the reference line is always smaller anywhere along the z-axis than at the origin. This is illustrated in figure 8 for the case of an ionization front that is assumed to be moving with a fixed curvature. We add that this observation should, in general, hold true for any wave front with a curvature that is non-flat, provided that the space charge density is maximum at the center.

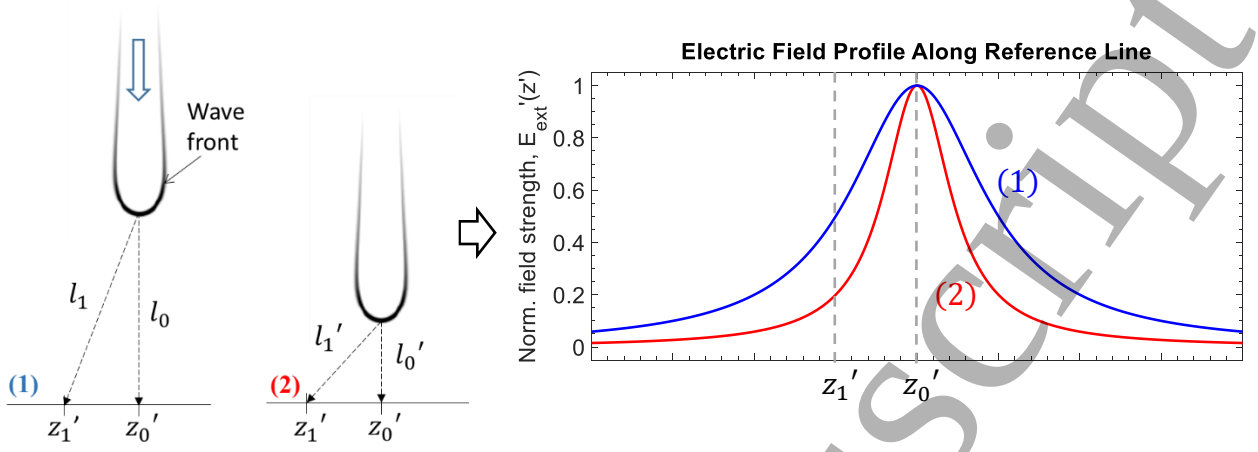

Figure 8. Illustration of the hypothesis behind the reduction in field (half) width with time. Left panel: consider a point on the z-axis, z_1', a fixed distance from the origin located at the axial centerline, z_0' or $(z' = 0)$. As the displacement, l, decreases from l_0 to l_0', the corresponding reduction in l_1 to l_1' is less. Right panel: since $E_{\text{ext}}'(z') \propto \frac{1}{l^2}$, this implies that the increase in the field $E_{\text{ext}}'(z' = z_1')$ is less than that of $E_{\text{ext}}'(z_0')$. The normalized electric field profile therefore reduces in width as the front approaches the z-axis.

This trend of decreasing (half) field width, a, coupled with the observation that the electric field profile may be accurately expressed using equation (6), provides a method for predicting the evolution of the field shape during *phase one*. A viable approach towards estimating or optimizing the measurement accuracy would be to predict the E-FISH modification factor as a function of a, by applying the analytical form of $E_{\text{ext}}'(z')$ in equation (3). This can be performed for an appropriate value(s) of the non-dimensional parameter, u, as captured in figure 9, bearing in mind that the profile width, a, is anticipated to decrease over time with respect to its Laplacian phase value, a_{L}. This approach is outlined in more detail in the following paragraph and demonstrates the importance of being able to accurately describe the normalized field profile, $E_{\text{ext}}'(z')$, with an analytical function.

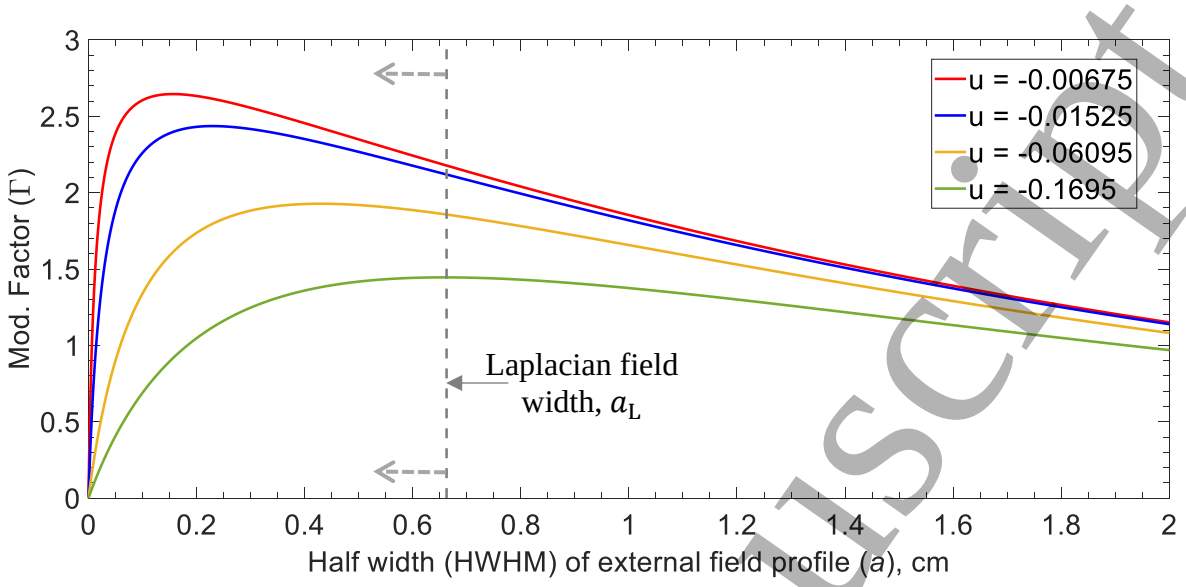

Figure 9. Plot of the E-FISH modification factor as a function of the field profile half width for $x_d = 5$ mm, HV case. The initial (Laplacian) field width, a_L, is represented by a grey vertical dashed line, and the expected change (drop) in a as the discharge evolves in time during the first phase is indicated by grey dashed arrows.

A suggested procedure would be to begin by computing the exact analytical function for the Laplacian electric field profile, based on equation (6). A sample best-fit curve, $E_{ext}'(z')$, for the HV case at $x_d = 5$ mm is shown in figure 10(a) with fit parameters $a = 0.66$ cm, and $b = 1.85$. Having established the analytical form of this initial field profile, the E-FISH modification factor, Γ, may be predicted as a function of the field width, a, while keeping b constant. The value of $u = \Delta k \cdot z_R$, can either be chosen so as to match the conditions of a previous experiment for obtaining an *estimate* of the E-FISH accuracy, or, to *optimize* the accuracy of an intended experiment. In the latter case, the objective is to seek an optimum u that minimizes changes in Γ relative to its Laplacian value Γ_L – that is, following equation (5), $\left(\frac{\Gamma}{\Gamma_L}\right) = \frac{(E_o)_{meas}}{(E_o)_{true}} \approx 1$ – over the most probable range of resulting field widths. This optimum value of u can in turn guide the selection of optical parameters such as the probe laser wavelength (Δk) or the choice of focusing (z_R).

In the absence of a reliable lower bound to the reduction in the profile field (half) width, a_{min}, an evident limitation of this approach is that only the sign of the error is known, and not its actual magnitude. (We address this issue in greater detail in section 7.) Nonetheless, as a preliminary verification, we use the values of a_{min} obtained from the simulations to validate this approach. Figures 10(b) and 10(c) plot the normalized E-FISH modification factor, $\left(\frac{\Gamma}{\Gamma_L}\right)$, as a function of the normalized profile field width, $\left(\frac{a}{a_L}\right)$, for two different conditions using the procedure described above. For each of these cases ($x_d = 5$ mm, HV case & $x_d = 3$ mm, LV case), the smallest field profile (half) width attained during the discharge evolution, based on figures 7(b) and 7(c), is found to be 40% and 10% respectively of its initial (or Laplacian phase) value, a_L. Based on these numbers ($\left(\frac{a}{a_L}\right) = 0.4$ & 0.1), the optimum values of u are -0.06095 & -0.1695 for figure 10(b),

and $u = -0.01525$ for figure 10(c). These values of u correspond to E-FISH modification factors, Γ, which exhibit minimum sensitivity with respect to their Laplacian field values, Γ_L, as the field profile (half) width, a, drops (i.e. as the discharge evolves with time) during the first phase. The normalized E-FISH modification factor, $\left(\frac{\Gamma}{\Gamma_L}\right)$, remains consistently close to unity, or more specifically, within the range $0.9 \lesssim \left(\frac{\Gamma}{\Gamma_L}\right) \lesssim 1.1$, indicating a measurement accuracy of 90%.

These optimum values of u are in excellent agreement with the results shown earlier in figure 5, thereby confirming the validity of this approach. In contrast with the results in figure 5, which are generated based on the electric field profiles from the plasma simulations, we stress that these predictions in figures 10(b) and 10(c) require no other input from these simulations apart from the minimum profile (half) width, $a_{\min}$.

Another important idea conveyed by the results in figures 10(b) and (c) is that the E-FISH accuracy in phase one depends strongly on the deviation between the field profiles of the plasma, and those of the Laplacian phase – the larger the extent of this deviation, the poorer the expected accuracy. This explains the better overall accuracy (with respect to u) of the results obtained for the HV case versus the LV case as highlighted earlier for figure 5. As reflected in figure 10(b), the overall variation in the normalized E-FISH modification factor, is predicted to remain within $0.8 \lesssim \left(\frac{\Gamma}{\Gamma_L}\right) \lesssim 1.2$ (corresponding to a measurement accuracy of 80%), compared with figure 10(c) where this figure drops to as low as 40%. The main reason is that the field profile (half) width experiences a significantly larger reduction in the LV case relative to its initial value. Evidence of these differences in reduction can be seen in figures 7(b) and 7(c), and also in figures 1(a) and 1(b). Based on the above idea, it is therefore expected that the E-FISH accuracy will decline sharply at axial (x) locations approaching the plane electrode. Not only is the Laplacian electric field profile much wider near the plane than at the pin electrode, but the field profile of the discharge also exhibits a significant narrowing in this region as displayed in figure 1(a). In other words, the disparity between the Laplacian electric field profiles and that of the plasma is anticipated to be amplified in the vicinity of the plane electrode.

On a relevant note, owing to a variation in the Laplacian field profile (and in particular, a_L) at different locations within the interelectrode gap – for instance as a function of x – this means that the most suitable choice of u may differ for different experimental conditions. This may introduce the need for multiple sets of calibration experiments.

Lastly, it is of interest to note that the curves in figures 10(b) and 10(c) are in fact, very similar. The slight difference lies with the analytical expression of the Laplacian electric field profile, $E_{\text{ext}}{}'(z) = \frac{1}{1+\left|\frac{z}{a}\right|^b}$ used to compute these curves. The value of b is 1.85 in figure 10(b) and for figure 10(c) it is 1.64 (a is the variable). That the resulting curves appear almost identical provides evidence of the insignificant influence of parameter b.

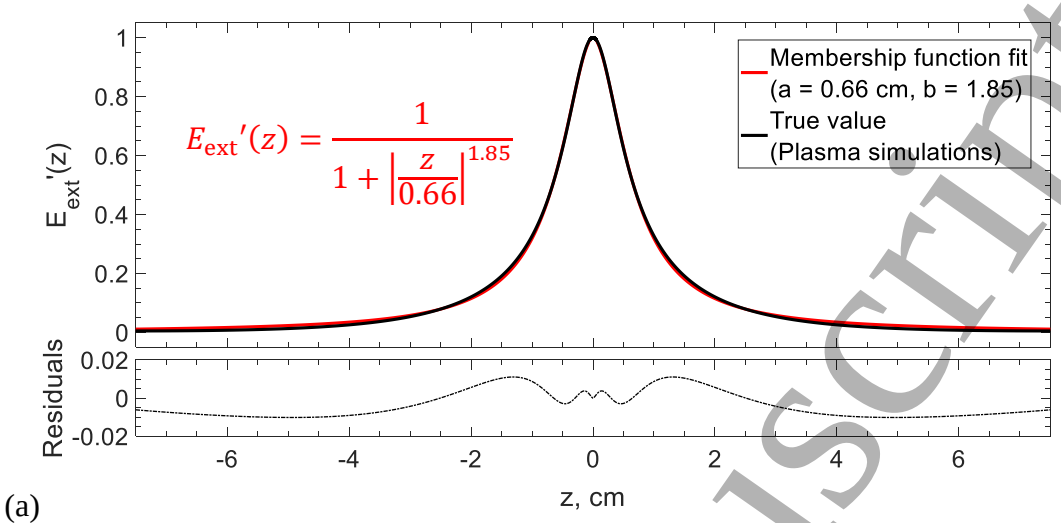

(a)

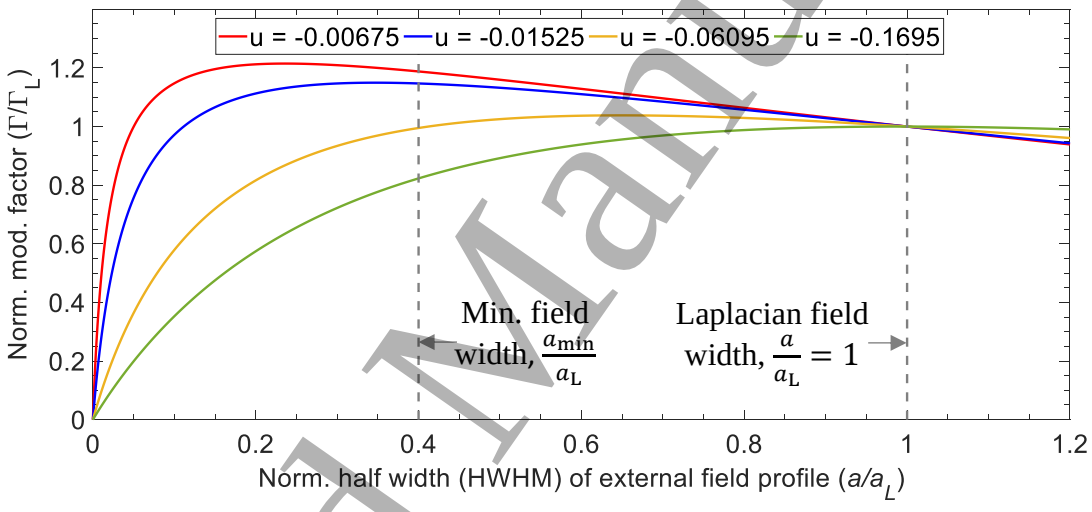

(b)

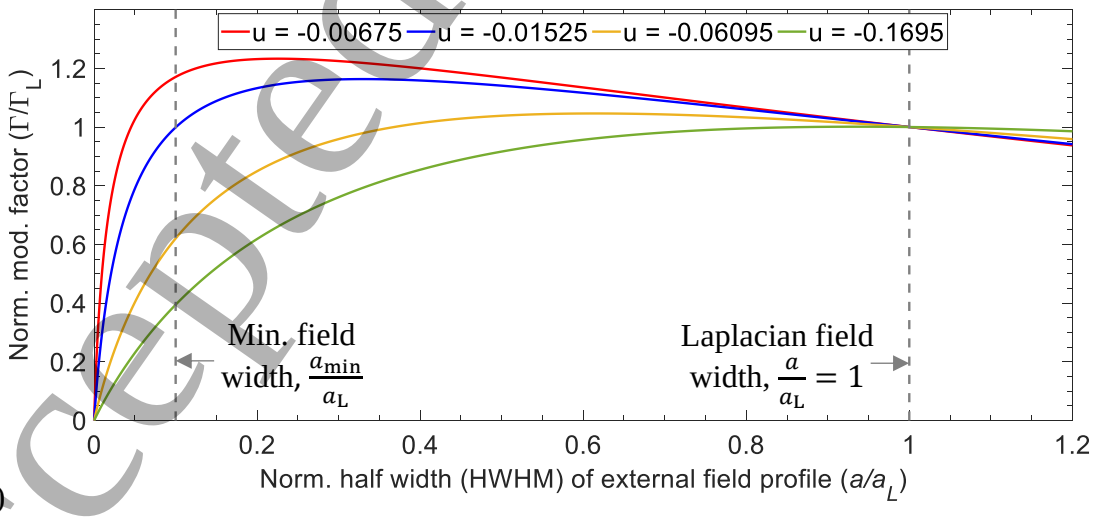

(c)

Figure 10. (a) Best fit curve to the Laplacian electric field profile along the z-axis based on equation (6) for the HV case at $x_d = 5$ mm. (b) Plot of the normalized E-FISH modification factor, as a function of normalized profile half width for optimizing the accuracy of the HV case at $x_d =$

5 mm. (c) Same as (b) but for the LV case at $x_{\mathrm{d}} = 3$ mm. Note that based on equation (5), $\left(\frac{\Gamma}{\Gamma_{\mathrm{L}}}\right) \lesseqgtr 1 \Rightarrow \frac{(E_o)_{\mathrm{meas}}}{(E_o)_{\mathrm{true}}} \lesseqgtr 1$. The range of field profile widths attained by the discharge lies between the two vertical, grey dashed lines.

7. Considerations for Future Use

One of the main contributions of this work, as discussed in sections 4 and 5, is to highlight the importance of the E-FISH modification factor in determining the accuracy of an E-FISH measurement. Following equation (3), the accuracy of the E-FISH modification factor may in turn be broken down into a few components. The parameter that has been fundamentally addressed in this work is the normalized field profile, $E_{\mathrm{ext}}{}'(z)$. In that respect, whether the group of radial profiles described in section 3 are a unique characteristic of this discharge, or perhaps a more standard feature of ionization waves, remains to be experimentally determined, but that similar field profiles have been observed for two different applied voltages suggests they are at least physically reasonable. Furthermore, we are encouraged that the results in figure 2 (time evolution of electric field profile) and figure 3 (radial profiles) are in good agreement with that recorded in the experimental literature [9,18].

Apart from the E-FISH modification factor for the plasma, section 6 underlines the elevated importance of accurately predicting the Laplacian electric field, so as to arrive at a sound estimate of its corresponding modification factor, Γ_{L}. This places an added emphasis on accurately modeling both the electrode (viz. pin) geometry as well as the attendant boundary conditions. From a broader perspective, the choice of the Laplacian electric field as the reference condition is not mandatory, and it is conceivable in certain problems, that a different, or even *multiple*, reference points could be used. In other words, there could exist other (multiple) time instants during the discharge where the normalized electric profile is known a priori and incorporating this information into the analysis could lead to a more precise bound on the E-FISH accuracy.

The other parameter in equation (3) which should not be overlooked is the laser Rayleigh range – a good measurement of z_{R} is implied. This can be realized by either using a beam profiler [27], or inferred by translating a knife edge perpendicular to the direction of beam propagation [28] and measuring the resulting beam intensity.

It should also be noted that the results derived in this work have assumed that the focal point of the laser coincides exactly with the discharge centerline (i.e. $r = 0$). Care should be taken during an experiment to ensure that this condition is fulfilled. Two plausible ways of achieving this could be to image the focal region of the laser beam using laser Rayleigh scattering, or to acquire an E-FISH signal profile along the z-axis by translating the laser focus with respect to the discharge set-up (for e.g. under Laplacian conditions).

The emphasis of this work has been on analyzing the effect of the electric field profiles on the E-FISH signal, and it has been assumed that the parameters such as, $\alpha^{(3)}$, the nonlinear hyperpolarizability, N, the neutral number density, and $P_{\mathrm{o}}^{(\omega)}$, the probe laser power, in equation (1) remain constant throughout the discharge. More generally however, the validity of this

assumption should be evaluated where possible. Accounting for changes in the laser intensity (or power) can be relatively straightforward, whereas effects such as a change in gas temperature or composition, affecting N and $\alpha^{(3)}$ respectively, are often more subtle, and can be much trickier to quantify.

7.1 Determining the Minimum Width of the Electric Field Profile, $a_{\min}$

As pointed out in section 6, the procedure for determining the E-FISH accuracy in phase one can be rendered fully independent of the plasma simulations provided an estimate of $a_{\min}$ can be either theoretically or experimentally established. One possibility is to acquire optical emission images from a high-lying atomic or molecular energy level populated by the plasma, and estimate $a_{\min}$ based on the radius of curvature of the discharge/ionization front. Such an approach demands further validation, but seems plausible given that similar approaches have been widely adopted in the literature. As an example, in N_2 plasmas, the emission intensity from the first negative system of N_2^+ and/or second positive system of N_2 could be used to provide a rough estimate of the electric field profile. The accuracy of such a procedure can be further assessed by numerically simulating the corresponding emission profiles as demonstrated in [37] and comparing them with experiments.

7.2 Measurements of Radial Field Component, E_r

The E-FISH diagnostic is capable of distinguishing between the different components of the electric field vector, as discussed in section 4. And though the present analysis focuses on the axial component, E_x, it is in principle, equally possible to measure the radial field, E_r, by monitoring its matching component of the E-FISH signal polarization. The accuracy of such measurements can then likewise be assessed by examining the effects of their corresponding field profiles, as we have done in this work. A note of caution is that, at least for axisymmetric geometries, the profile of E_r along the z-axis is likely to be peaked away from the axial centerline since the field at the centerline is necessarily zero. Given the non-intuitive nature of the signal response for such profiles (for e.g. the double-peak profiles described in section 5), analyzing the E-FISH accuracy for E_r could be comparatively more challenging, and may require a more carefully conceived calibration configuration. The effect of any possible change in the sign of E_r along the laser path on the E-FISH signal also merits further examination.

8. Conclusion

The effect of the electric field profile (in a plasma) on the E-FISH signal has been examined in the specific case of atmospheric pressure, nanosecond discharges for a pin to plane geometry. Two slightly different geometries and applied voltages have been studied. In the HV case, a 5mm/ns ionization front propagating in the gap and producing a diffuse discharge with a conical shape at its connection to the grounded cathode and in the LV case, a discharge with a smaller and more constant radius as it propagates in the gap. To assess this effect on the measurement accuracy, we theoretically predict the outcome of an E-FISH experiment, using the electric field profiles from numerical simulations as the true values. We formally quantify this accuracy in terms of an E-FISH modification factor, which is a function of both the shape of the field profile, and a non-

dimensional factor, u, defined as the product of the wave vector mismatch, Δk, and the Rayleigh range of the focused laser beam, z_R.

Three distinct electric field profile shapes are observed from these simulations, corresponding to an initial phase before the arrival of the ionization wave, an intermediate phase exhibiting a double-peaked or annular profile after the passage of the wave, and a third or final phase when the interelectrode gap is closed, forming a conductive channel as the discharge transitions to a quasi-steady state. In this respect, the effect of applied voltage is secondary, although the LV case simulations result in a much narrower discharge.

Expectedly, the overriding factor for determining the E-FISH accuracy is the difference between the instantaneous electric field profile of the plasma, and the chosen reference value (in this work, the Laplacian electric field profile). The larger this deviation, the poorer the accuracy. More specifically, it is found that field profiles that are peaked away from the axial centerline tend to produce a more inaccurate E-FISH measurement – the more pronounced this difference between the peak field strength and the value at the centerline, the more inaccurate the measurement.

In line with these ideas, we generally find that the predicted E-FISH signal is closer to the true (simulated) field values for the first and third phases, with much larger discrepancies noted for the second phase. Since the electric field strengths in the first phase are the highest, the *shape* of the time evolution curve for the peak-normalized electric field displays relatively good agreement with their true values. This could partially explain why existing E-FISH measurements have often yielded plausible results. Likewise, the HV case plasma simulations, which display a comparatively smaller change in the electric field profile during the discharge evolution relative to its Laplacian phase, generally produce more accurate results in comparison with the LV case. This highlights the importance of not over-generalizing the results for a particular applied voltage.

Moving beyond understanding the effect of the electric field profiles on the E-FISH accuracy to *predicting* this accuracy, requires knowledge of how the electric field profiles evolve over time – a significantly more challenging task. We focus our efforts on the first phase of the ionization wave development, where it is noticed that the width of the electric field profile constricts gradually, while maintaining an almost similar shape to that of its Laplacian conditions. We find consistent evidence, both physically and numerically, to suggest that this behaviour is a fundamental feature, at least for this class of discharges. On the premise of this assumption, we propose an approach towards estimating and optimizing the accuracy of an E-FISH measurement during this initial phase of the discharge.

We believe that a similar approach could be sought for other types of discharges to understand how E-FISH performs, with a view to consequently improving the measurement accuracy. Likewise, a better characterization of the attendant field profiles, especially in the second and final phases of the present discharge, using analytical approaches for instance, could also provide further insight into the E-FISH accuracy during these later stages. Overall, these findings point favourably towards the continued use of the E-FISH diagnostic.

Acknowledgments

The work was partially supported by the French General Directorate of Armaments (DGA) under the EP-DGA convention N2790, the French National Research Agency, ANR ("Atomic Species Production via Electronically excited states in high eNergy density Plasmas" (ASPEN) Project) and the French–Russian international Research Project KaPPA 'Kinetics and Physics of Pulsed Plasmas and their Afterglow'. The 2D fluid simulations presented in this work have been performed thanks to the computational resources of the cluster Hopper at Ecole Polytechnique.

References

1. Bigio, I. J., Finn, R. S., & Ward, J. F. (1975). Electric-field induced harmonic generation as a probe of the focal region of a laser beam. *Applied optics*, *14*(2), 336-342.
2. Dogariu, A., Goldberg, B. M., O'Byrne, S., & Miles, R. B. (2017). Species-independent femtosecond localized electric field measurement. *Physical Review Applied*, *7*(2), 024024.
3. Goldberg, B. M., Reuter, S., Dogariu, A., & Miles, R. B. (2019). 1D time evolving electric field profile measurements with sub-ns resolution using the E-FISH method. *Optics letters*, *44*(15), 3853-3856.
4. Chng, T. L., Naphade, M., Goldberg, B. M., Adamovich, I. V., & Starikovskaia, S. M. (2020). Electric field vector measurements via nanosecond electric-field-induced second-harmonic generation. *Optics Letters*, *45*(7), 1942-1945.
5. Goldberg, B. M., Chng, T. L., Dogariu, A., & Miles, R. B. (2018). Electric field measurements in a near atmospheric pressure nanosecond pulse discharge with picosecond electric field induced second harmonic generation. *Applied Physics Letters*, *112*(6), 064102.
6. Simeni, M. S., Tang, Y., Frederickson, K., & Adamovich, I. V. (2018). Electric field distribution in a surface plasma flow actuator powered by ns discharge pulse trains. *Plasma Sources Science and Technology*, *27*(10), 104001.
7. Chng, T. L., Orel, I. S., Starikovskaia, S. M., & Adamovich, I. V. (2019). Electric field induced second harmonic (E-FISH) generation for characterization of fast ionization wave discharges at moderate and low pressures. *Plasma Sources Science and Technology*, *28*(4), 045004.
8. Cui, Y., Zhuang, C., & Zeng, R. (2019). Electric field measurements under DC corona discharges in ambient air by electric field induced second harmonic generation. *Applied Physics Letters*, *115*(24), 244101.
9. Chng, T. L., Brisset, A., Jeanney, P., Starikovskaia, S. M., Adamovich, I. V., & Tardiveau, P. (2019). Electric field evolution in a diffuse ionization wave nanosecond pulse discharge in atmospheric pressure air. *Plasma Sources Science and Technology*, *28*(9), 09LT02.
10. Huang, B., Zhang, C., Adamovich, I., Akishev, Y., & Shao, T. (2020). Surface ionization wave propagation in the nanosecond pulsed surface dielectric barrier discharge: the influence of dielectric material and pulse repetition rate. *Plasma Sources Science and Technology*, *29*(4), 044001.
11. Orr, K., Tang, Y., Simeni, M. S., van den Bekerom, D., & Adamovich, I. V. (2020). Measurements of electric field in an atmospheric pressure helium plasma jet by the E-FISH method. *Plasma Sources Science and Technology*, *29*(3), 035019.

12. Meehan, K. C., Starikovskiy, A., & Miles, R. (2020). Two component electric field dynamics of a ns-SDBD plasma with sub-nanosecond resolution by femtosecond EFISH. *AIAA Scitech 2020 Forum* (p. 1747).
13. Orr, K., Yang, X., Gulko, I., & Adamovich, I. V. (2020). Formation and propagation of ionization waves during ns pulse breakdown in plane-to-plane geometry. *Plasma Sources Science and Technology*, *29*(12), 125022.
14. Rousso, A. C., Goldberg, B. M., Chen, T. Y., Wu, S., Dogariu, A., Miles, R. B., Kolemen, E., & Ju, Y. (2020). Time and space resolved diagnostics for plasma thermal-chemical instability of fuel oxidation in nanosecond plasma discharges. *Plasma Sources Science and Technology*, *29*(10), 105012.
15. Butterworth, T. D., & Cha, M. S. (2021). Electric field measurement in electric-field modified flames. *Proceedings of the Combustion Institute*, *38*(4), 6651-6660.
16. Cui, Y., Wang, H., Zhuang, C., Luo, H., Wang, X., & Zeng, R. (2020). Electric field measurement in dielectric barrier discharges using electric field induced second harmonic generation in ambient air. *IEEE Transactions on Dielectrics and Electrical Insulation*, *27*(6), 2071-2077.
17. Lepikhin, N. D., Luggenhölscher, D., & Czarnetzki, U. (2020). Electric field measurements in a He: N2 nanosecond pulsed discharge with sub-ns time resolution. *Journal of Physics D: Applied Physics*, *54*(5), 055201.
18. Huang, B., Zhang, C., Zhu, W., Lu, X., & Shao, T. (2021). Ionization waves in nanosecond pulsed atmospheric pressure plasma jets in argon. *High Voltage*, *6*(4), 665-673.
19. Chng, T. L., Starikovskaia, S. M., & Schanne-Klein, M. C. (2020). Electric field measurements in plasmas: how focusing strongly distorts the E-FISH signal. *Plasma Sources Science and Technology*, *29*(12), 125002.
20. Feng, S., & Winful, H. G. (2001). Physical origin of the Gouy phase shift. *Optics letters*, *26*(8), 485-487.
21. Levy, U., & Silberberg, Y. (2015). Second and third harmonic waves excited by focused Gaussian beams. *Optics express*, *23*(21), 27795-27805.
22. Takashima, K., Adamovich, I. V., Xiong, Z., Kushner, M. J., Starikovskaia, S., Czarnetzki, U., & Luggenhölscher, D. (2011). Experimental and modeling analysis of fast ionization wave discharge propagation in a rectangular geometry. *Physics of Plasmas*, *18*(8), 083505.
23. Klochko, A. V., Starikovskaia, S. M., Xiong, Z., & Kushner, M. J. (2014). Investigation of capillary nanosecond discharges in air at moderate pressure: comparison of experiments and 2D numerical modelling. *Journal of Physics D: Applied Physics*, *47*(36), 365202.
24. Lepikhin, N. D., Popov, N. A., & Starikovskaia, S. M. (2018). Fast gas heating and radial distribution of active species in nanosecond capillary discharge in pure nitrogen and N_2: O_2 mixtures. *Plasma Sources Science and Technology*, *27*(5), 055005.
25. Vandalon, V., & Kessels, W. M. M. (2021). Influence of the spatial extent of the space-charge region in c-Si on the electric-field-induced second-harmonic-generation effect. *JOSA B*, *38*(6), 1840-1849.
26. http://researchhubs.com/post/maths/fundamentals/bell-shaped-function.html
27. Standard, I. S. O. (2005). 11146,"*Lasers and laser-related equipment–test methods for laser*

beam widths, divergence angles and beam propagation ratios."

28. Siegman, A. E. (1993). Defining, measuring, and optimizing laser beam quality. In *Laser Resonators and Coherent Optics: Modeling, Technology, and Applications* (Vol. 1868, pp. 2-12). International Society for Optics and Photonics.
29. Bourdon, A., Péchereau, F., Tholin, F., & Bonaventura, Z. (2021). Study of the electric field in a diffuse nanosecond positive ionization wave generated in a pin-to-plane geometry in atmospheric pressure air. *Journal of Physics D: Applied Physics*, *54*(7), 075204.
30. Naidis, G. V., Tarasenko, V. F., Babaeva, N. Y., & Lomaev, M. I. (2018). Subnanosecond breakdown in high-pressure gases. *Plasma Sources Science and Technology*, *27*(1), 013001.
31. Babaeva, N. Y., & Naidis, G. V. (2021). Universal nature and specific features of streamers in various dielectric media. *Journal of Physics D: Applied Physics*, *54*(22), 223002.
32. Kulikovsky, A. A. (1997). Positive streamer between parallel plate electrodes in atmospheric pressure air. *Journal of physics D: Applied physics*, *30*(3), 441.
33. Kulikovsky, A. A. (1998). Positive streamer in a weak field in air: A moving avalanche-to-streamer transition. *Physical Review E*, *57*(6), 7066.
34. Chng, T. L., Naphade, M., Goldberg, B. M., Adamovich, I. V., & Starikovskaia, S. M. (2020). Electric field vector measurements via nanosecond electric-field-induced second-harmonic generation. *Optics letters*, *45*(7), 1942-1945.
35. Zhu, Y., Chen, X., Wu, Y., Hao, J., Ma, X., Lu, P., & Tardiveau, P. (2021). Simulation of the ionization wave discharges: a direct comparison between the fluid model and E--FISH measurements. *Plasma Sources Science and Technology*, *30*(7), 075025.
36. Hansen, L., Goldberg, B. M., Feng, D., Miles, R. B., Kersten, H., & Reuter, S. (2021). Energy transfer in interaction of a cold atmospheric pressure plasma jet with substrates. *Plasma Sources Science and Technology*, *30*(4), 045004.
37. Bonaventura, Z., Bourdon, A., Celestin, S., & Pasko, V. P. (2011). Electric field determination in streamer discharges in air at atmospheric pressure. *Plasma Sources Science and Technology*, *20*(3), 035012.
38. Babaeva, N. Y., & Naidis, G. V. (1996). Two-dimensional modelling of positive streamer dynamics in non-uniform electric fields in air. *Journal of Physics D: Applied Physics*, *29*(9), 2423.
39. Anikin, N. B., Starikovskaia, S. M., & Starikovskii, A. Y. (2002). Polarity effect of applied pulse voltage on the development of uniform nanosecond gas breakdown. *Journal of Physics D: Applied Physics*, *35*(21), 2785.
40. Sorokin, D. A., Beloplotov, D. V., Tarasenko, V. F., & Baksht, E. K. (2021). Main modes of runaway electron generation during a breakdown of high-pressure gases in an inhomogeneous electric field. *Applied Physics Letters*, *118*(22), 224101.
41. Hoder, T., Šimek, M., Bonaventura, Z., Prukner, V., & Gordillo-Vázquez, F. J. (2016). Radially and temporally resolved electric field of positive streamers in air and modelling of the induced plasma chemistry. *Plasma Sources Science and Technology*, *25*(4), 045021.
42. Jahanbakhsh, S., Hoder, T., & Brandenburg, R. (2019). Correlation between electric field, current and photon emission in subsequent barrier corona microdischarges. *Journal of Applied Physics*, *126*(19), 193305.

43. Hoder, T., Loffhagen, D., Voráč, J., Becker, M. M., & Brandenburg, R. (2016). Analysis of the electric field development and the relaxation of electron velocity distribution function for nanosecond breakdown in air. *Plasma Sources Science and Technology*, *25*(2), 025017.